UNCLASSIFIED

Australian Government
Department of Defence
Science and Technology

Benchmarking the AMC Cavitation Tunnel for Hydrodynamic Measurements on Submarine Models with CFD Determined Blockage Corrections

Daniel Butler[1], David B. Clarke[1], Chris L. Ellis[2], Paul Brandner[2] and Mohammed Kandoussi[3]

[1]Maritime Division
Defence Science and Technology Group

[2]Australian Maritime College
University of Tasmania

[3]Ministry of Defence
United Kingdom

DST-Group-TR-3358

ABSTRACT

The widely studied generic submarine hull form SUBOFF was used to benchmark the use of the Australian Maritime College's (AMC) cavitation tunnel for hydrodynamic measurements on submarine models. The measurements acquired at the AMC cavitation tunnel are a subset of those taken at the David Taylor Research Centre (DTRC), allowing direct comparison. The measurements were performed on a 1.54 m model for Reynolds numbers between 8 and 18 million. The measurements included surface pressure, skin friction, boundary layer velocities and a wake survey on the bare hull at zero degrees incidence. The large scale of the model relative to the tunnel resulted in a blockage ratio of 8.1%. The results were corrected using correction factors determined from Computational Fluid Dynamics (CFD) simulations, and displayed a high level of agreement with the DTRC results. The positive comparison showed that the AMC facility could be used for models of this size when combined with CFD based blockage corrections.

RELEASE LIMITATION
Approved for public release

UNCLASSIFIED

Produced by

Maritime Division
Defence Science and Technology Group
506 Lorimer Street
Fishermans Bends, Victoria, 3207, Australia

Telephone: 1300 333 362

Copyright Commonwealth of Australia 2017
April 2017
AR-016-836

APPROVED FOR PUBLIC RELEASE

Benchmarking the AMC Cavitation Tunnel for Hydrodynamic Measurements on Submarine Models with CFD Determined Blockage Corrections

Executive Summary

The generic submarine hull form SUBOFF was used to benchmark submarine model testing in the Australian Maritime College's (AMC) cavitation tunnel. For this series of measurements only the bare hull with and without the aft control surfaces was used.

The cavitation tunnel's test section is 2.6 m long, with a 600 x 600 mm cross section. It can operate with flow speeds of between 2 and 12 m/s. The model was held at a constant zero degrees incidence for the duration of these measurements. The 180 mm diameter model and support foils resulted in a solid blockage ratio of 8.1%.

Measurements taken included the surface pressure and skin friction on the bare hull at a range of Reynolds numbers between 8 and 18 million. Boundary layer velocity profiles were calculated from total and static pressure probe measurements obtained using a 3D traverse at a number of locations around the aft of the bare model for a Reynolds number of 12 million. The unsteady velocity component was also calculated to obtain the turbulence intensity at these locations. Wake velocity measurements were obtained at the aft of both the bare hull and the partially appended model.

The relatively high blockage ratio necessitated a correction method to allow comparisons with measurements made at other facilities. These corrections were generated with the aid of Computational Fluid Dynamics (CFD) simulations.

The corrected measurements showed good agreement with results obtained at the David Taylor Research Centre's (DTRC) Anechoic Flow Facility. DTRC measurements were made with a smaller solid blockage ratio (3.5%). In general the results showed that measurements in the cavitation tunnel, with blockage corrections, are accurate and reliable for this scale of model. The wake survey results did show a small discrepancy which may warrant further investigation.

This work was conducted as part of the SEA 1000 Submerged Wakes and Propeller Hydrodynamics work package (PRP.3, deliverable 8 and HYD.8, deliverable 2).

This page is intentionally blank.

Authors

Daniel Butler
Maritime Division

Daniel Butler is hydrodynamics researcher employed by DST, prior to 2107 he was employed in the same role as a contractor through the University of Tasmania. He obtained his Bachelors in Engineering (Mechanical and Aerospace) with 1st class Honours in 2012 from the University of Queensland. Prior to commencing tertiary studies he obtained a trade certificate and worked as a maintenance fitter and draftsman for 5 years. Since 2013 he has been working in the DST Group's Hydroacoustics Science and Technology Capability on the SEA 1000 project. This work has included model testing, data analysis, and design of experimental equipment. He has played a major role in the development of the Digital Image Correlation photogrammetry capability in the AMC cavitation tunnel.

David B. Clarke
Maritime Division

David Clarke commenced work in the Maritime Operations Division (MOD) at DST Group in 1988 after completing a Bachelor of Science at the University of Sydney. His work in MOD focused on magnetic sensors and instrumentation. He obtained a Graduate Diploma in Computer Engineering from RMIT in 1996. In 1998 he joined the Maritime Platforms Division to specialise in the hydrodynamics of underwater vehicles. His work on underwater vehicles encompasses experimental, empirical, and computational hydrodynamics. The experimental work was conducted at the University of Tasmania's cavitation tunnel where he played a major role in developing the instrumentation and techniques used in this laboratory. In 2009 he completed a Ph.D. at the University of Tasmania examining transcritical flow past ellipsoids. He completed a long term attachment to Maritime Research Insitute Netherlands (MARIN) computing flows around maneouvering vessels in 2011 after being awarded a Defence Science Fellowship. Recently he has lead a small team studying flow around submarines and their appendages in support of the SEA 1000 project.

Chris L. Ellis
University of Tasmania

Chris Ellis is a contractor working for DST Group funded bythe SEA 1000 program. He is employed by the Australian Maritime College, within the University of Tasmania. He obtained a double Bachelor degree in Engineering (Mechanical) and Technology (Aerospace) from Monash University in 2006. After this, he entered service with the Australian Army and served as the Technical Support Platoon commander within 6th Battalion, The Royal Australian Regiment until Jan 2007 where he moved onto 2/14 Light Horse Regiment (Queensland Mounted Infantry) as the Technical Support Troop commander. He left the Army in mid 2008 and began a Ph.D. at Monash University in 2009. He completed the Ph.D. in 2012 and began working for the Hydroacoustics Science and Technology Capability in January 2013 under the SEA 1000 project in experimental and computational fluid mechanics.

Paul A. Brandner
University of Tasmania

Paul Brandner is an Associate Professor of hydrodynamics at the Australian Maritime College (AMC), a specialist institute of the University of Tasmania. He is Research Leader and facility Manager of the Cavitation Research Laboaratory (CRL) at AMC. He obtained a Bachelor of Engineering with Honours (1991) and a Ph.D. (1996) from the University of Tasmania. He has worked in Naval Hydrodynamics since 1991 and from 1996 has specialised in cavitation. He led the development of the CRL from 2001 funded under the AusIndustry Major National Facilities Program. He has developed a long term collaboration with DST Group as a major stakeholder of the CRL and its involvement in the SEA 1000 project.

Mohammed Kandoussi
Ministry of Defence (UK)

Mohammed graduated from the University of Newcastle with an Master of Engineering in Naval Architecture and is currently working for the Ministry of Defence (MoD) in the UK. Working with the MoD provided Mohammed with the opportunity to be exposed to the maritime industry. He traveled to different countries and had multiple secondments, one of them in Australia working for the Defence and Science Technology Group; where he was part of the hydroacoustics group. His work was to assess the blockage effect in the Australian Maritime college (AMC) cavitation tunnel and its effect on the tests results using Computational Fluid Dynamic (CFD). Currently, Mohammed is working in service support within the Warship support team responsible for amphibious ships including the Landing Platform Helicopter (LPH), HMS Ocean*; Landing Platform Docks (LPD), HMS* Albion *and* Bulwark*; Landing Craft Vehicle and Personnel (LCVP) and Landing Craft Utility (LCU) which operate from LPH and LPD.*

This page is intentionally blank.

Contents

This page is intentionally blank.

Nomenclature

C_p	Pressure coefficient $\left(\frac{P-P_{s\infty}}{q}\right)$
C_f	Skin friction coefficient $\left(\frac{\tau_w}{q}\right)$
I	Turbulence intensity
L	Model length, m
P_s	Static pressure (including surface pressure), Pa
P_t	Total pressure $(P_s + q)$
P_{tube}	Preston tube stagnation pressure, Pa
q	Dynamic pressure $\left(\frac{1}{2}\rho U_\infty^2\right)$, Pa
r, R_s, R_{max}	Radius, local surface radius, maximum surface radius, m
Re	Reynolds number $\left({}^{UL}/_{\nu}\right)$ based on hull length
s_{frpp}	Sensitivity of the fast response pressure probe, Pa/V
$\bar{u}, u'$	Local velocity magnitude, fluctuating component of velocity, m/s
U_∞	Inlet velocity magnitude, m/s
$(u)_{max}$	maximum velocity magnitude in the x/L plane, m/s
u_τ	Friction velocity $(\sqrt{\tau_w/\rho})$, m/s
x	Streamwise location, origin at tip of hullform bow, m
$y+$	Viscous wall distance coefficient $\left(\frac{yu_t}{\nu}\right)$
ΔC_p	Surface pressure correction offset
ρ	Density, kg/m^3
σ	Standard deviation
τ_w	Wall shear stress, Pa
ν	Kinematic viscosity, m^2/s
φ	azimuthal angle, °

Nomenclature

Subscripts

i	"ith" measurement location
CFD	Computed results
corrected	Corrected results
free	Measurement in flow field with negligible viscous loss due to model
LB	Low blockage CFD domain
max	Maximum value normal to the body axis from a given location on the surface
measured	Measured result
ref	Reference measurement location
tunnel	AMC cavitation CFD domain
x, y, z	Directional components
∞	Conditions at test section or domain inlet

Abbreviations

AFF	Anechoic Flow Facility (at DTRC)
AMC	Australian Maritime College
DTRC	David Taylor Research Centre (USA)

1. Introduction

Accurate simulation of the flow field surrounding a submarine is critical for understanding the flow around the control surfaces and propeller. These flows impact the propeller's loading, efficiency and acoustic signature as well as the effectiveness of the control surfaces. A critical step in attaining confidence in flow simulations is comparison with accurate experimental data.

Measurements about the generic submarine body "SUBOFF" (Groves et al. 1989) have been undertaken at the Australian Maritime College's (AMC) Cavitation Tunnel to benchmark the facility for submarine model testing. This facility is well suited to studying submarine appendages but minimal work has been undertaken on full submarine models, prompting this benchmarking study. The generic profile of the SUBOFF model has been used extensively for computational and experimental fluid dynamics studies, making it a suitable tool for benchmarking and facility comparison (Groves et al. 1989; Haung et al. 1989).

The SUBOFF model in the cavitation tunnel's test section resulted in a solid blockage ratio of 8.1%. This blockage influenced the flow conditions and needs to be accounted for to allow comparisons with results obtained in other facilities. Computational Fluid Dynamics (CFD) simulations were performed for a geometry representative of the SUBOFF model in the AMC cavitation tunnel test section and on the model in a low blockage domain. Comparing the results from these simulations allow an accurate, full body blockage correction to be made, allowing the calculation of the effective open water results.

This report presents measurement methods, results, blockage corrections and uncertainty estimates for the SUBOFF model tested in the AMC cavitation tunnel. The corrected measurements are then compared to results obtained from other facilities. These measurement methods and corrections have also been applied to the Joubert generic submarine model (Clarke et al. 2016).

2. Cavitation Tunnel Description

The AMC cavitation tunnel is a closed circuit variable pressure water tunnel (Figure 1 and Figure 2). All wet surfaces of the AMC cavitation tunnel are constructed from stainless steel. The tunnel can operate at a range of pressures from 4 kPa to 400 kPa absolute. The test section cross section is 0.600 m wide for its full length and 0.600 m high at the entrance of the 2.60 m long test section. The bottom surface of the test section has a 0.44° slope to compensate for boundary layer growth to achieve streamwise velocity uniformity. The test section has a height at its exit of 0.620 m.

The test section employs removable acrylic or stainless steel side windows and a stainless steel top window. These windows have a range of flush access points that allow for mounting of models or experimental apparatus.

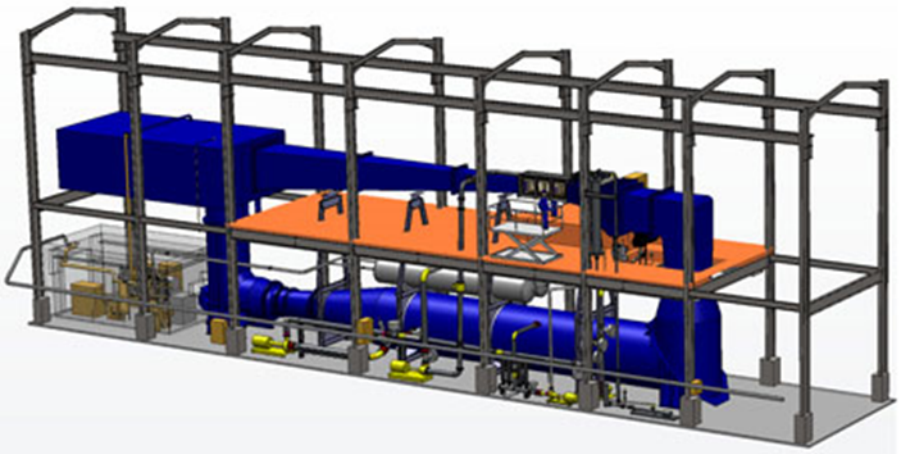

Figure 1: CAD image of the AMC cavitation (Brandner et al. 2007)

The tunnel is driven by a 200 kW main pump and is capable of speeds ranging from 2 m/s (minimum speed required for water bearings in the pump to function correctly) up to 12 m/s. This allows Reynolds numbers (based on the width of the test section) of the order of 10^6 to be achieved. The tunnel volume is 365 m^3 and is filled with demineralised water.

The AMC cavitation tunnel is instrumented to measure test section static and dynamic pressures, water temperature and dissolved gas content. The data from these sensors are used to calculate and control the tunnel mean velocity or Reynolds number, in addition to the static pressure or cavitation number.

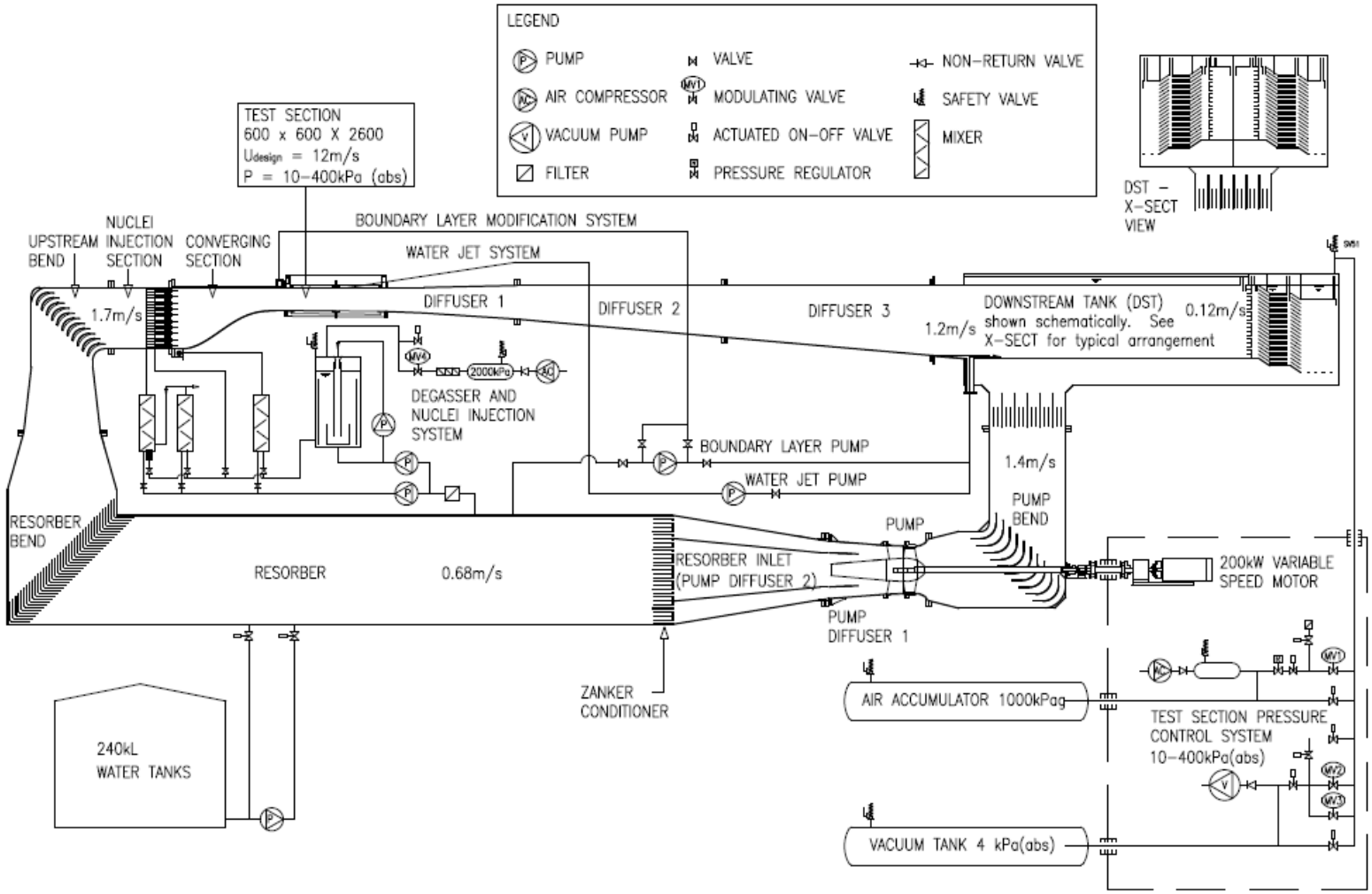

Figure 2: Schematic of the cavitation tunnel facility (Brandner et al. 2007)

3. Model Description

The SUBOFF model geometry was created by the David Taylor Research Centre (DTRC) as a generic submarine shape that could be freely shared for the purpose of comparing and validating CFD models. Experimental and CFD data has been published for this geometry from a number of international organisations. The measurement types and measurement locations for this work program were selected to allow direct comparison with data obtained in the DTRC's Anechoic Flow Facility (AFF) (Haung et al. 1989). The geometry is described by Groves et al. (1989). This work mainly examined the 'bare hull' configuration without the fin (sail) or aft control surface. A small number of measurements were repeated with the aft control surfaces fitted.

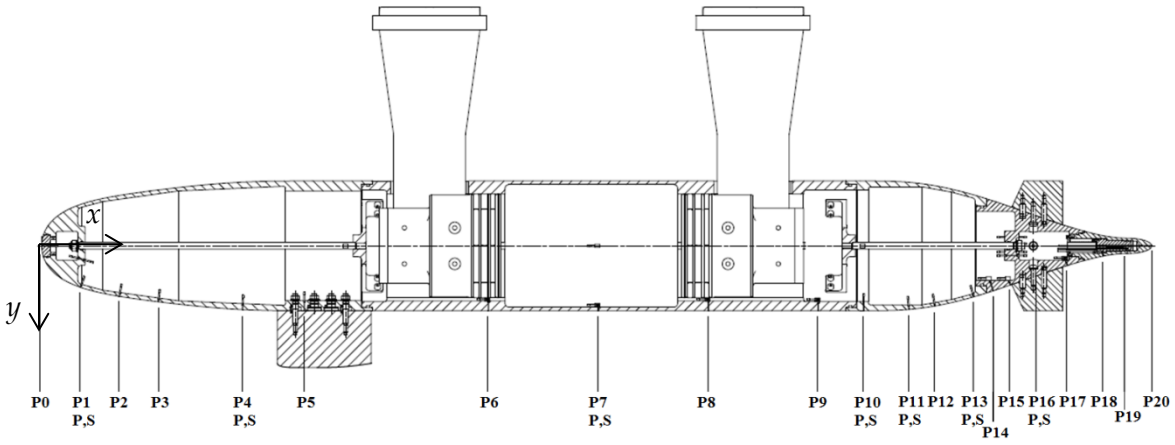

Figure 3: Fully appended DST Group SUBOFF model as mounted in the test section from the top window. Body fixed coordinate system shown with origin at the bow. P,S denotes locations of port and starboard pressure tappings.

The DST Group SUBOFF model (Figure 3) was manufactured from grade 6061 aluminium. The finished model was anodised and had a surface roughness of less than 0.8 µm. The model was mounted in the AMC cavitation tunnel test section upside down as shown in Figure 3 by two tapered NACA0016 foils. The model configuration tested was axisymmetric so the orientation is arbitrary but, for consistency with any future work, the complete model's ordinate directions are used. A clamp arrangement between the foil and submarine allows the model to be orientated and translated over a small range of incidences and vertical positions. The model had a length, L, of 1543.5 mm and a maximum radius, R_{max}, of 90 mm. The model centreline was raised 20 mm from the test section centre line to allow greater wall clearance if the fin (sail) was fitted. All measurements taken in this study were at zero degrees incidence. The model was fitted with an adhesive dot trip strip at x/L=0.05 (faintly visible in

Figure 4). The trip strip was designed to stimulate transition to a turbulent boundary layer for Reynolds numbers larger than 9.3×10^6 with minimum flow disturbance. The desired

trip height determined for x/L=0.05 at this Reynolds Number was 102 µm. The trip strip height was selected from the nearest suitable commercially available material. The trip dots were cut 1.25 mm diameter from 95 µm thick self-adhesive PVC sheet and placed at 2.5 mm centres.

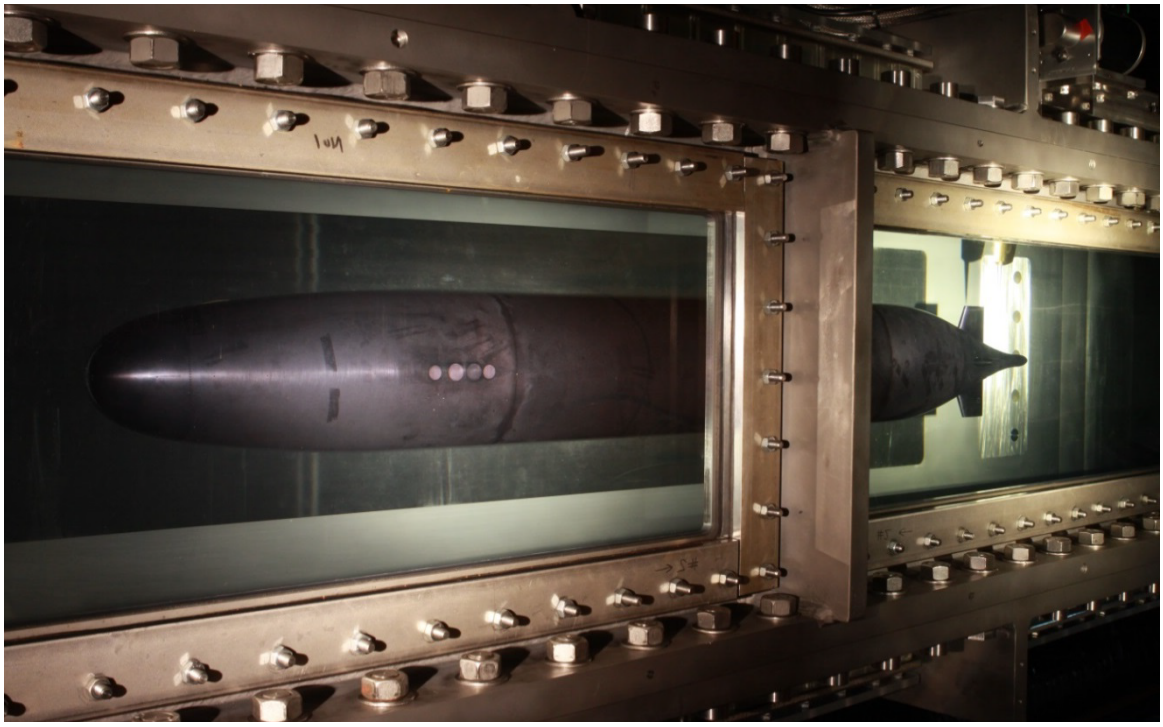

Figure 4: SUBOFF with aft control surfaces in the AMC cavitation tunnel (viewed from below the test section).

4. Experimental Setup and Procedure

These measurements consisted of surface pressure and skin friction measurements at a range of Reynolds numbers on the bare hull, as well as boundary layer velocity surveys on the bare hull at a Reynolds number of 12×10^6, and wake velocity surveys on the bare and partially appended hull also at a Reynolds number of 12×10^6. When present the aft control surfaces were at 0° incidence.

4.1 Surface pressure

The DST Group SUBOFF model is fitted with 35 surface pressure tappings, 21 opposite the support foils and 7 each on the port and starboard sides (Figure 3). They are drilled perpendicular to the surface and at similar *x/L* locations to the original DTRC model. These tappings are connected via a scanning valve to a Validyne DP15-42 differential pressure transducer located outside of the tunnel and referenced to the free-stream static pressure. Data was sampled at 1024 Hz for 10 s to obtain a mean pressure coefficient defined in Equation (1).

$$C_p = \frac{\overline{P - P_{s\infty}}}{\bar{q}_\infty} \tag{1}$$

Where P is the surface pressure, $P_{s\infty}$ is the free-stream static pressure and q_∞ is the inlet dynamic pressure.

4.2 Skin friction

The static pressure ports were fitted with a streamlined fairing to mount a Preston tube. The skin friction was calculated from that measurement using Head and Ram's calibration (Head & Ram, 1971).

$$C_f = \frac{\tau_w}{q_\infty} = \frac{f(\bar{P}_{Tube} - \bar{P}_s)}{\overline{q_\infty}} \tag{2}$$

Where τ_w is wall shear stress, P_{Tube} is pressure measured by the Preston tube and P_s is surface pressure.

This calibration returns the wall shear stress as a function of the pressure difference between the Preston tube and the local surface pressure (Equation (2]). Head and Ram do not provide any guidance on the calibrations usage on axisymmetric bodies. It is reasonable to assume that the calibration is appropriate whilst the local hull radius is much larger than the Preston tube and that the boundary layer in the immediate vicinity of the Preston tube follows the law of the wall.

The Preston tubes were manufactured from a 0.5 mm diameter thin walled hypodermic stainless steel tube and adhesively mounted via a streamlined plastic fairing. The plastic fairings were mounted over the surface pressure tappings (Figure 5). This mounting technique induces a small inaccuracy in position as the Preston tube measurement location is displaced 10 mm upstream of the location where the surface pressure measurement is

taken. This error is significantly reduced by interpolating the surface pressure measurement to the location at the tip of the Preston tube. The streamlined plastic fairings were manufactured from acrylic using a 3D printer with a resolution of 16 µm.

Figure 5: Preston tube and fairing (top, dimension in mm) and Preston tubes in place on a tail cone segment (bottom).

4.2.1 Upstream disturbances and repeatability

The time consuming nature of applying and resetting Preston tubes in a cavitation tunnel compelled the use of multiple tubes during a single test run. Placing a second Preston tube downstream of another was avoided as much as possible. The streamlined design of the Preston tube fairings minimised the wake allowing some tubes to be placed inline, provided there was sufficient downstream separation. The disturbing influence of an upstream Preston tube was studied over a number of runs. The study was performed by comparing measurements performed with a Preston tube upstream of another Preston tube at varying distances to those obtained with no upstream obstruction.

The application of the tubes is time consuming due to the mechanical complexity of operations in a cavitation tunnel and the need to adhesively mount the Preston tubes. The

additional density of the fluid provides greater pressures than those obtained in a low speed wind tunnel, giving greater signal to noise ratio.

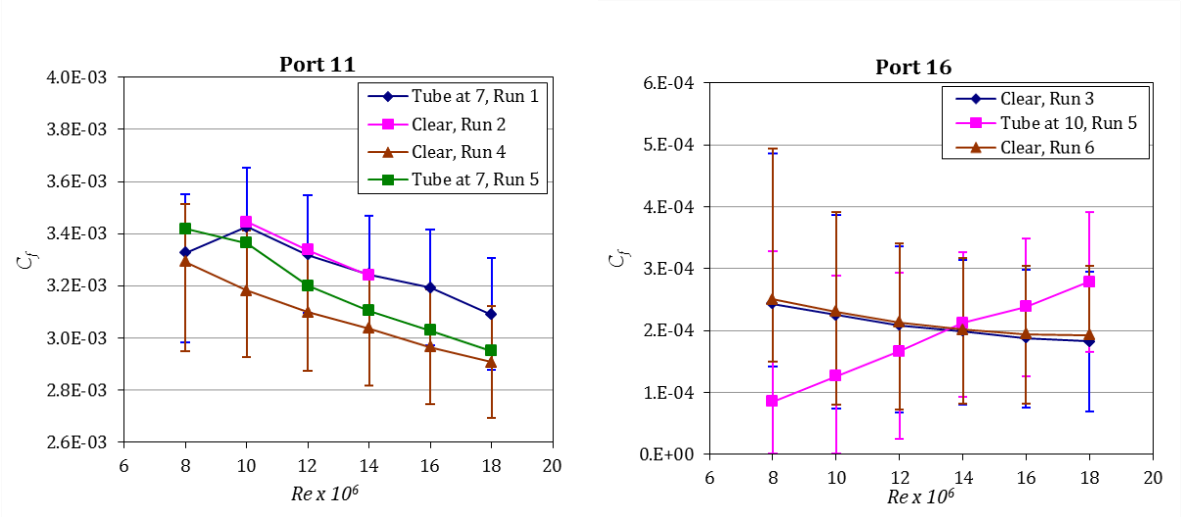

Figure 6: Skin friction measurements at ports 11 & 16 with and without an upstream Preston tube

Figure 6 shows the measured skin friction for a number of locations with and without a Preston tube upstream. Port 11 is 551 mm downstream of Port 7 and shows little sign of interference from the Preston tube at Port 7 (Figure 6, left). A small variation is seen between runs 1, 2 and 4, 5 from reapplying the Preston tube between runs 2 and 4. Generally this demonstrates that the technique is more sensitive to the application of the Preston tube than it is to the upstream disturbance. Port 16 is 270 mm downstream of Port 10 (Figure 6, right). The upstream disturbance clearly has an effect on the reading at Port 16, though the effect is still well within the bounds of uncertainty. The smallest separation used for two inline Preston tube measurements in this report was 549 mm.

4.3 Velocity measurements

Flow velocity was calculated from fast response pressure probes (Clarke, 2009) positioned by an automated 3D traverse mounted to the side of the test section (Figure 7). Measurements were taken at the same locations in turn with a static and a total pressure probe head, featuring a 0.7 mm probe tip aligned with the test section axis (x direction). The probe head housed an Entran EPB-B01-7B-Z2 pressure transducer, measuring the pressure differential between the probe tip and the tunnel free-stream static pressure. The mean non-dimensionalised velocities were calculated from these two pressure measurements using Equation (3).

$$\frac{u_{x,i}}{U_\infty} = \sqrt{\left(\frac{P_{t,i} - P_{s,ref}}{q}\right) - \left(\frac{P_{s,i} - P_{s,ref}}{q}\right)} \qquad (3)$$

Where $u_{x,i}$ is the flow velocity at point i, U_∞ is the inlet velocity, $P_{t,i}$ is the total pressure at point i, $P_{s,i}$ is the static pressure at point i and $P_{s,ref}$ is the probes reference static pressure at the test section wall.

The fast response total pressure probe enabled the measurement of turbulent fluctuations. For the velocity surveys all probe measurements were taken at a Reynolds number of 12×10^6 for 20 s with a 16.384 kHz sampling rate. This is equivalent to approximately 100 flow passes over the model at a sampling rate well above the maximum expected frequency content. The output of the fast response total pressure probe was filtered using a low pass, single pole Bessel filter with a cut-off frequency of 2 kHz. The low pass filter was used to remove the resonance peak that occurs at 4.2 kHz due to the interaction of the pressure sensor diaphragm and the water in the probe tip. The unsteady velocity was computed as the standard deviation of the velocity,

$$\frac{u'_{x,i}}{U_\infty} = \frac{\left(u_{x,i} - \bar{u}_{x,i}\right)_{rms}}{U_\infty} = \sigma\left(\frac{u_{x,i}}{U_\infty}\right) \tag{4}$$

where $\left(u_{x,i} - \bar{u}_{x,i}\right)$ is the instantaneous unsteady velocity, $u'_{x,i}$ is the root mean square of the unsteady velocity and σ is the standard deviation.

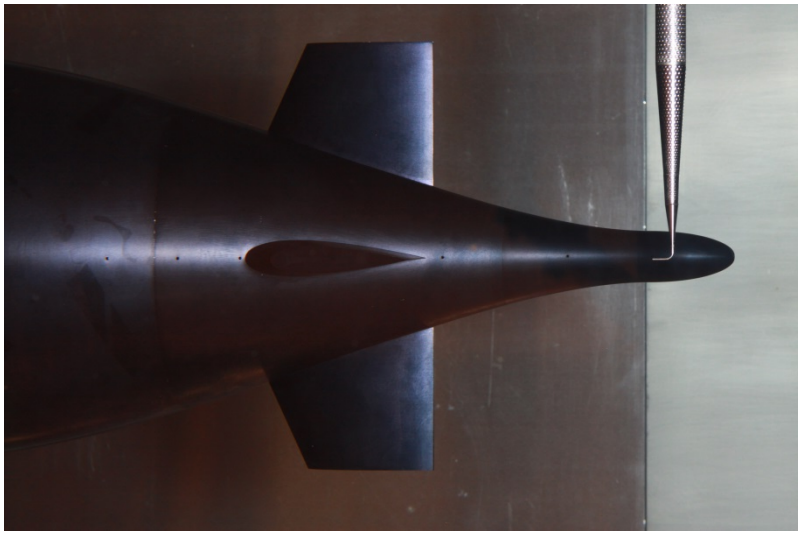

Figure 7: Fast response pressure probe taking measurements in the wake. Shown from below.

4.3.1 Boundary layers

The boundary layer velocities were determined at x/L=0.904, 0.927, 0.956 and 0.978. Two sets of boundary layer measurements were obtained; one with the measurement locations along an axis normal to the submarine axis and a second on an axis normal to the submarine local surface (Figure 8, left). For all measurements the distance r-R_s refers to the total distance from the surface point to the measurement location. Measurements were taken on a plane 135° from the support. This minimised the disturbing influence of the

supporting foils and allowed the probe to travel further out into the free-stream, as the test section has an approximately square cross section.

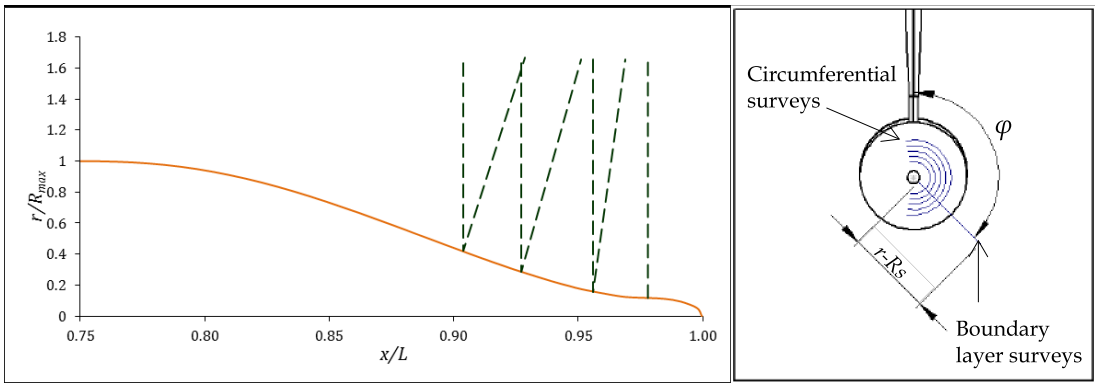

Figure 8: Boundary layer survey axial locations (left). Boundary and circumferential survey locations on the bare model in the test section (right)

The static pressure was recorded to within 8 mm of the model surface ($[r-R_s]/R_{max}$ approx. 0.09). Static measurements closer to the surface were avoided to minimise error in the measurement due to the influence of the wall. In the case of x/L=0.978, the static measurement had plateaued when approaching 8 mm distance from the wall. This allowed an assumption of constant static pressure for the remaining points in this set. Circumferential surveys were made at x/L=0.978 along 5 arcs centred on the submarine's axis (Figure 8, right). Each arc constituted 98 measurement locations with a freestream reference before and after the arc.

5. CFD Simulations

The measurements in the AMC cavitation tunnel were subject to greater blockage than the measurements in the DTRC AFF. Computational Fluid Dynamic (CFD) simulations were used to assess the influence of blockage on measurements (Ellis et al. 2015). These CFD simulations predicted the flow around the SUBOFF model in the AMC cavitation tunnel and in larger reduced blockage domains (Table 1).

Table 1: Computational domain dimensions

	Length (mm)	Width (mm)	Height (mm)	Blockage ratio
AMC tunnel test section	7660 (4.96 L)	600 (6.67 R_{max})	600	8.1%
Small low blockage domain	7660 (4.96 L)	1250 (13.9 R_{max})	1250	1.9%
Large low blockage domain	7660 (4.96 L)	2500 (27.8 R_{max})	2500	0.47%

5.1 AMC cavitation tunnel domain

The AMC cavitation tunnel domain was based on the geometry of the AMC tunnel test section with a 600 x 600 mm inlet and sloping test section floor that dropped 20 mm over the 2.60 m length of the test section. The domain was extended 2.38 m (1.54 L) upstream of the test section and 2.68 m (1.74 L) downstream (Figure 9). The walls of the upstream domain were set as slip walls to prevent boundary layer growth. The walls in the test section and the downstream extensions of the domain used non-slip walls, allowing a smooth continuous boundary layer growth throughout the area of interest. The upstream and downstream extension to the test section minimises undesirable interaction between the model and the inlet and outlet boundary conditions respectively.

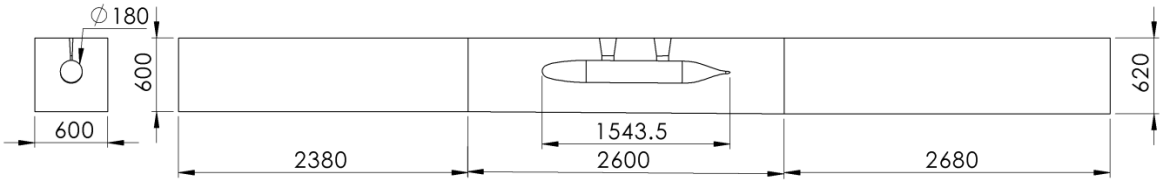

Figure 9: Computational domain for SUBOFF in the AMC tunnel test section, dimensions in mm

The simulations were performed using ANSYS Fluent. The incompressible formulation of the Reynolds-Averaged Navier-Stokes (RANS) equations was solved using the segregated solver. Second-order discretisation was selected for the continuity, momentum and turbulent variables. The SIMPLEC algorithm was selected for pressure-velocity coupling. The realisable k-ε turbulence model with enhanced near wall modelling was selected as it is the most suitable of the k-ε turbulence models for handling streamline curvature and

separation (Kim, 1999) and based on previous experience of performing CFD simulations of cavitation tunnel tests (Clarke, 2009).

The submarine model, with its support foils, was placed in the same location in the test section as during the experimental program. A structured mesh was created throughout the domain. The $y+$ values on the hull surface were generally in the range of 30 to 60. The maximum grading normal to the wall was 1.08. The inlet was modelled as a constant velocity inlet with the velocity set to give a Reynolds number of 12×10^6 and the turbulence intensity was set at 0.5%, which is comparable to the measured tunnel turbulence intensity. The outlet was set as an outflow.

5.2 Low blockage domains

Two domains with reduced blockage were created by expanding the walls of the AMC mesh outwards in the horizontal and vertical directions to approximate open water conditions. The cross section of the large low blockage domain was enlarged to 2500 x 2500 mm, reducing the blockage ratio to 0.47%. A second smaller low blockage domain was constructed with a cross section of 1250 x 1250 mm resulting in a solid blockage of ratio of 1.6%. This small low blockage domain was produced to examine the trend in results as the blockage ratio was modified. The large low blockage domain was constructed from an inner mesh (1250 x 1250 mm), featuring the hull and support foils, and an outer mesh (2500 x 2500 mm) (Ellis et al. 2015).

For both low blockage domains the support foils were extruded to the limits of the 1250 x 1250 mm domain (Figure 10). The surface of the extruded foils was set with a slip wall boundary condition. The outer walls of the low blockage domains were also set with a slip wall boundary condition. For the large low blockage domain (2500 x 2500 mm) a non-conformal interface was used corresponding to the extents of the small low blockage domain (1250 x 1250 mm). The support foils were not extended into the large low blockage domain to reduce the cell count in the larger domain. This is expected to have minimal influence on the simulated flow around the model due to the distance of the truncation from the model and the minimal impact of the support foil on the solid blockage ratio.

The low blockage domain simulations were performed with the same solver settings as the simulation of the SUBOFF model in the AMC cavitation tunnel test section. The large low blockage domain model reduced the free-stream velocity increase to a maximum of 0.30% at x/L=0.33.

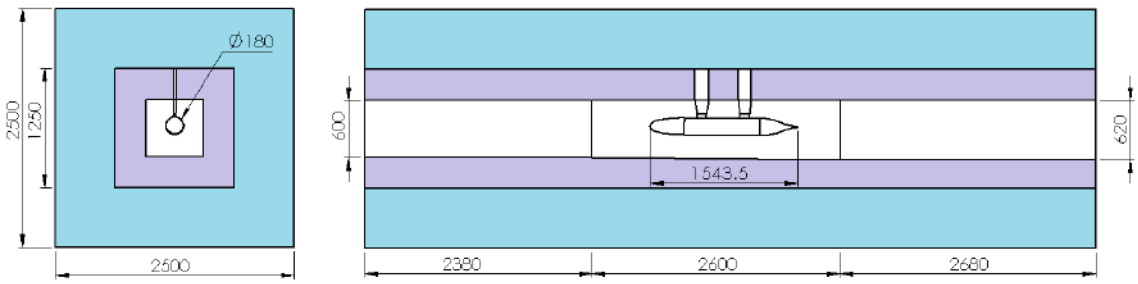

Figure 10: Low blockage domains, dimensions in mm

6. Comparative Results and Corrections

Surface pressure, skin friction and off body measurements around the stern obtained in the DTRC Anechoic Flow Facility are available for the SUBOFF model (Haung et al. 1989). These measurements are used as a reference for comparison with CFD and experimental results obtained in this project. DTRC measurements on the SUBOFF geometry were conducted at a larger scale than is possible in the AMC cavitation tunnel (Table 2) but with common Reynolds numbers.

Table 2: Model Dimensions

	DTRC	DST Group
Maximum Body Diameter (m)	0.508	0.180
L (total body length) (m)	4.356	1.544
Tunnel Cross Section (m)	2.44x2.44	0.6x0.6
Maximum Solid Blockage (Bare Hull at 0° incidence with support foils)	3.5%	8.1%

There are many techniques used for blockage correction ranging from the estimation of free-stream velocity change from geometric considerations and potential flow (Barlow et al. 1999); to the use of stream-wise pressure gradient measurements and reference velocities as used in DTRC's Anechoic Flow Facility (Haung et al. 1989); to the full body CFD simulations conducted for this study. Each is a compromise between accuracy and cost with both factors differing between facilities and test setups. Obtaining pressure gradient measurements on the walls of the AMC Cavitation Tunnel would be a difficult as it currently lacks suitable tapping locations. For this study CFD modelling was chosen as it is able to determine accurate blockage corrections and provide insight into the flow around the model at locations where no measurements were practical.

6.1 Surface pressures

Figure 11 shows the measured surface pressure distribution on the model's hull in the AMC cavitation tunnel together with those taken at DTRC. The offset between the two highlights the effect of the large blockage ratio.

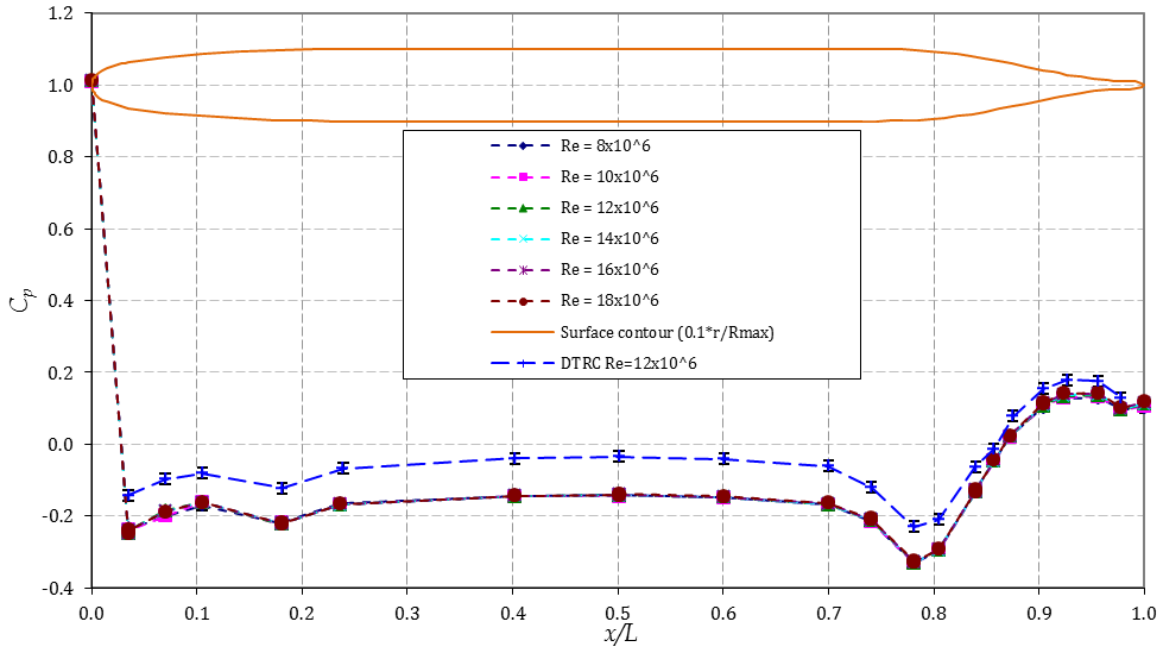

Figure 11: Surface pressure on the bare SUBOFF hull, uncertainty C_p±0.007.

Figure 12 shows the surface pressure (C_p) distributions at the bow of the model, across the range of Reynolds numbers. Their agreement indicates the trip strip, located at x/L=0.05, was successful in creating results that are essentially Reynolds number independent. There is a small Reynolds number dependence visible in Figure 12 between x/L=0.070 and 0.105 for the two lesser Reynolds numbers. This is due to an increase in the streamwise distance required to stimulate the transition to turbulence at the lower Reynolds numbers. The dependence is most probably due to the trip strip taking a greater distance to destabilise the laminar boundary layer at the lesser Reynolds number. The port and starboard measurements all fall within the bounds of error with no significant bias, indicating the model is correctly aligned with the flow (Appendix A.2).

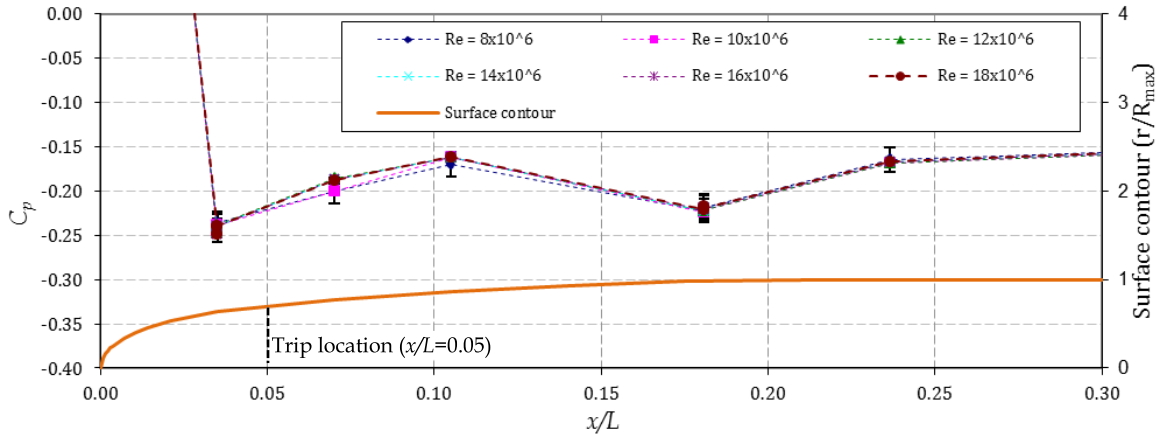

Figure 12: Surface pressure measurements at the bow of the SUBOFF model in the AMC tunnel.

Blockage corrections were determined from the comparison of CFD simulations of the SUBOFF model in the AMC tunnel test section and in the very low blockage conditions, (Equation (5]) (Ellis et al. 2015).

$$\Delta C_p = C_{p,LB} - C_{p,tunnel} \tag{5}$$

The computed and corrected surface pressure coefficient distributions are shown in Figure 13. The close agreement between the measurements without blockage correction and the computed surface pressure coefficient distribution for the SUBOFF model in the AMC tunnel domain provides confidence in using the CFD simulations for blockage correction. This correction accounts for both the static pressure drop and the velocity increase caused by the blockage. The estimated blockage correction, ΔC_p, is a function of surface position. The correction is applied to the measured surface pressure distribution for the centre-line tappings (Figure 13).

Figure 13 also presents results from the DTRC AFF which had also been blockage corrected to account for a small variation in the measured pressure coefficient distribution around SUBOFF model in the DTRC facility (Haung et al. 1989). These are in agreement with the corrected results obtained in the AMC tunnel.

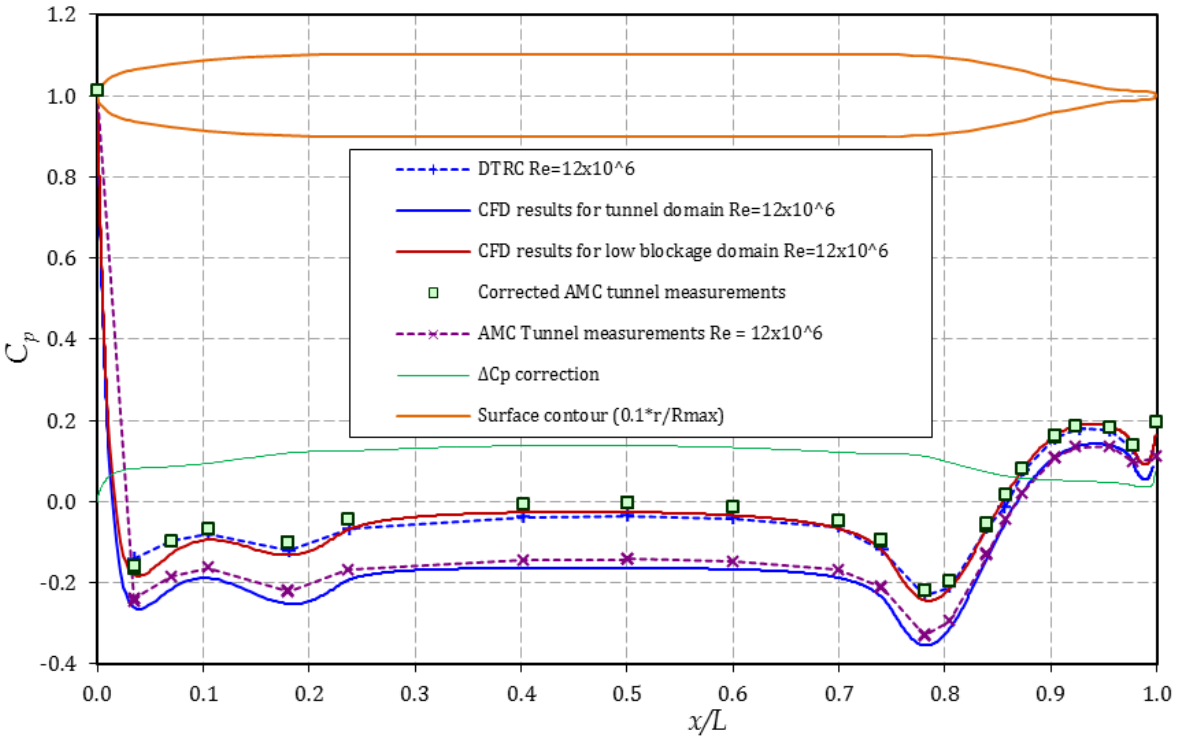

Figure 13: Calculated surface C_p distributions for the SUBOFF model at a Reynolds number of 12×10^6 in AMC and DTRC tunnels with CFD results and corrections. AMC measurement uncertainty C_p±0.007 (Appendix A.1), DTRC measurement uncertainty C_p±0.015.

6.2 Skin friction

The skin friction coefficients determined from the Preston tube measurements are shown in Figure 14. Measurements were not obtained for locations forward of Port 6 (x/L≈0.4) as the boundary layer momentum thickness there is insufficient to achieve reliable results with the size of Preston tube used.

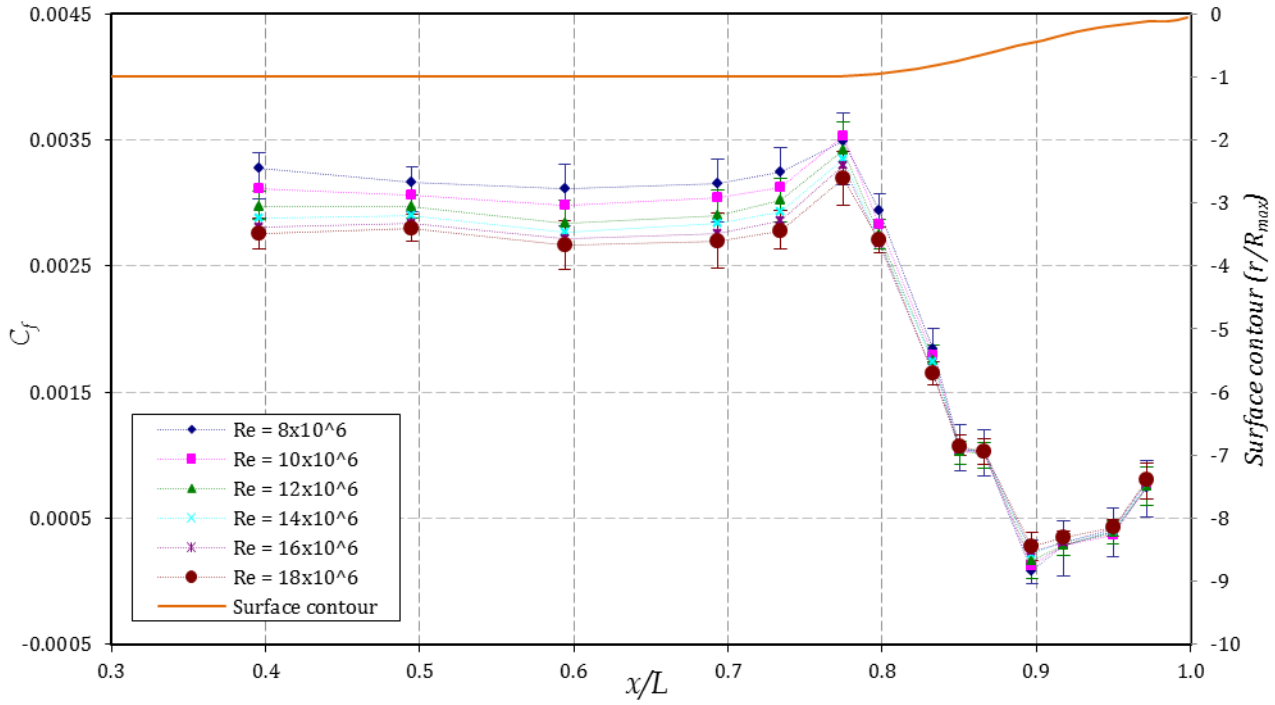

Figure 14: Skin friction measurements on the SUBOFF bare hull, not corrected for blockage.

The skin friction data was corrected by rescaling each measurement point based on the relative maximum dynamic pressure in each measurement plane (Equation (6]). The maximum dynamic pressure is typically the notional free stream.

$$C_{f,corrected} = \left(\frac{\tau_w}{q_\infty}\right)_{measured} \left(\frac{(u_{LB})_{max}}{(u_{tunnel})_{max}}\right)^2_{CFD} \qquad (6)$$

Where $(U)_{max}$ is the maximum velocity in the x/L plane corresponding to the location measured in the test section. The *measured* and *CFD* subscripts represent data collected from the tunnel or from the CFD models respectively.

In areas of high curvature the maximum dynamic pressure occurs closer to the body, and the resulting change in skin friction is different than what a free stream correction would predict. CFD based corrections allow this effect to be quantified and corrected. The correction, shown in Figure 15 as the ratio of dynamic pressures, reduces with the solid blockage to almost zero near the tail.

The blockage corrected data points are mostly within the bounds of uncertainty of the DTRC measurements. Points *x/L* = 0.798 and 0.890 are possibly in error as the results disagree with both the DTRC and CFD datasets by significantly more than the measurement uncertainty (see Figure 15). Similarly while the measurements at x/L=0.774 and 0.851 are relatively close to the CFD and DTRC results, if time had permitted a repeated measurement may have been warranted. This error can most likely be attributed to poor sealing around the Preston tube fairings, which would result in a lower skin friction value. Generally increased uncertainty can be expected in this region of rapidly varying hull diameter. This was the first attempt at using this design of Preston tube fairing and with the restricted time available it was not possible to retake those measurements. Subsequent tests have demonstrated improved results with a slightly modified fairing and greater experience (Clarke et al. 2016).

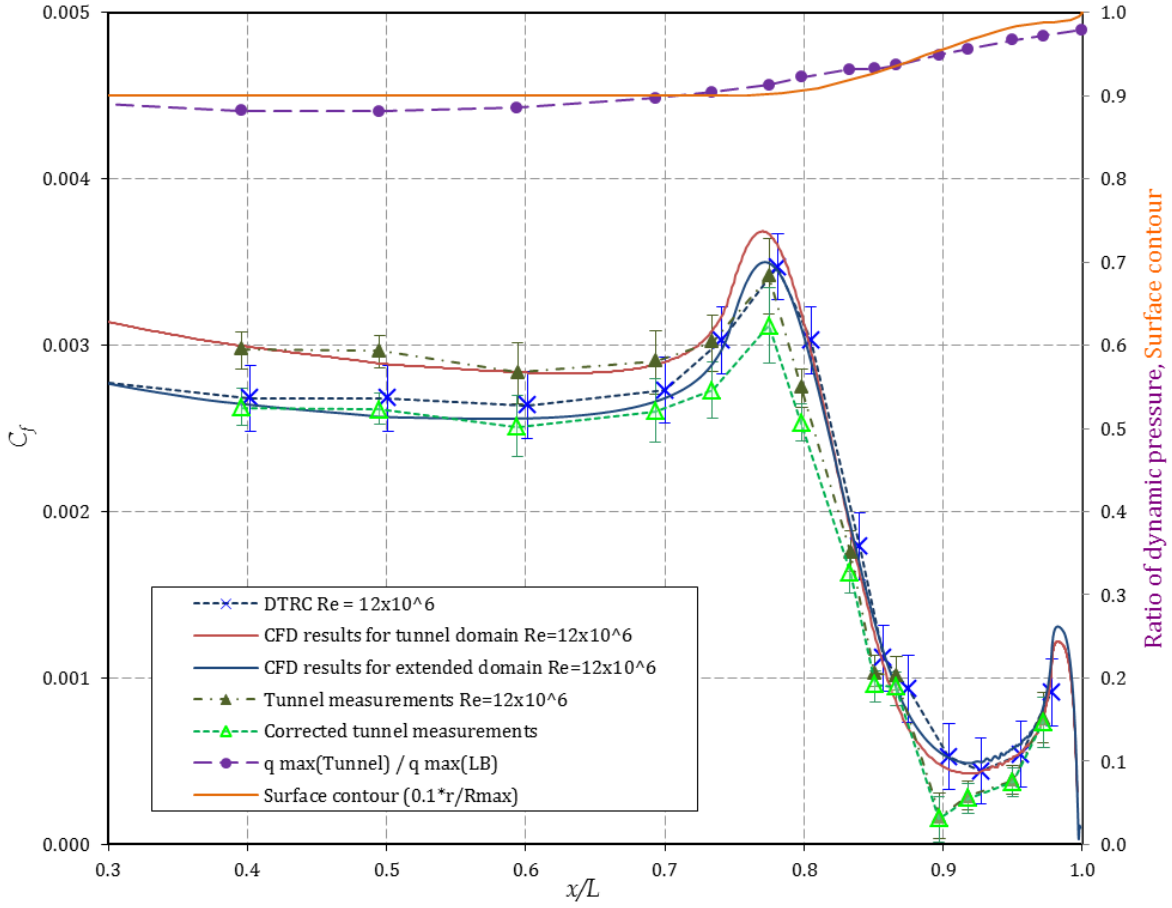

Figure 15: Skin friction measurements taken on the SUBOFF model at AMC tunnel relative to CFD and DTRC measurements (Haung et al. 1989) at Re=12×10^6. Uncertainty calculations shown in Appendix A.3

6.3 Boundary layer velocities

The boundary layer surveys are shown in Figure 16 and in Figure 18, the latter with a smaller radial range. The blockage affected measurements, non-dimesionlised by the test section inlet velocity, show negligible difference between the axis and surface normal data sets for the measured locations. The most common blockage correction for boundary layer velocities is to scale the measured velocities by the local free-stream velocity. In this series of measurements the presence of a streamlined probe support prevented the retraction of the probe into the free-stream.

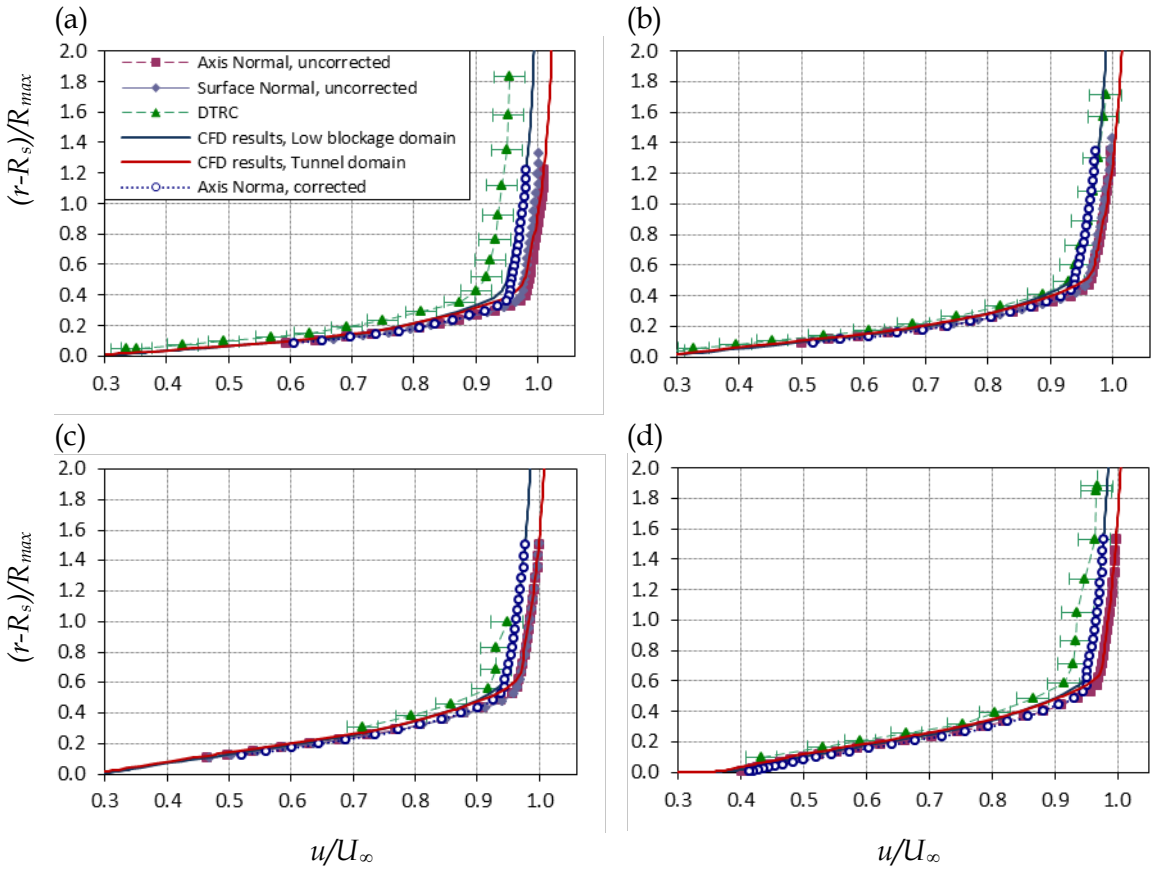

Figure 16: Normalised full boundary layer velocities on the SUBOFF model at x/L=0.904 (a), 0.927 (b), 0.956 (c) and 0.978 (d) with DTRC measurements (Haung et al. 1989) and CFD (Ellis et al. 2015) for Re=12×10^6. Measurement uncertainty u/U$_\infty$±0.014

The total pressure measurement reaches its free-stream value once the probe is withdrawn outside the flow influenced by viscous losses. This occurs for the SUBOFF model at the measured locations once $(r - R_s)/R_{max} > 0.9$ for even the thickest boundary layer measured (Figure 17). The total pressure reaches its free-stream value significantly closer to the hull than the velocity does due to the influence of the hull shape on the static pressure. A measurement of the total pressure obtained in the flow not influenced by the viscous losses may thus be used to obtain an updated sensitivity of the fast response

pressure probe, s_{frpp}. This is determined from the known dynamic pressure of the fluid at the entrance to the test section, q_∞, and the difference in static pressure between the entrance to the test section (P_{s_∞}) and the location used for the reference pressure ($P_{s_{ref}}$) for the fast response pressure probe,

$$s_{frpp} = \frac{P_{t_{free}} - P_{s_{ref}}}{V_{frpp}} = \frac{q_\infty + P_{s_\infty} - P_{s_{ref}}}{V_{frpp}} \tag{7}$$

Where V_{frpp} is the measured probe voltage and ($P_{t_{free}} - P_{s_{ref}}$) is the pressure difference between the tip of the total head probe and the probe's reference pressure, assuming the probe is located in a region of the flow where negligible viscous losses have occurred from the test sections entrance. For these measurements $\frac{P_{s_\infty} - P_{s_{ref}}}{q_\infty}$ was determined from CFD to be approximately 0.006.

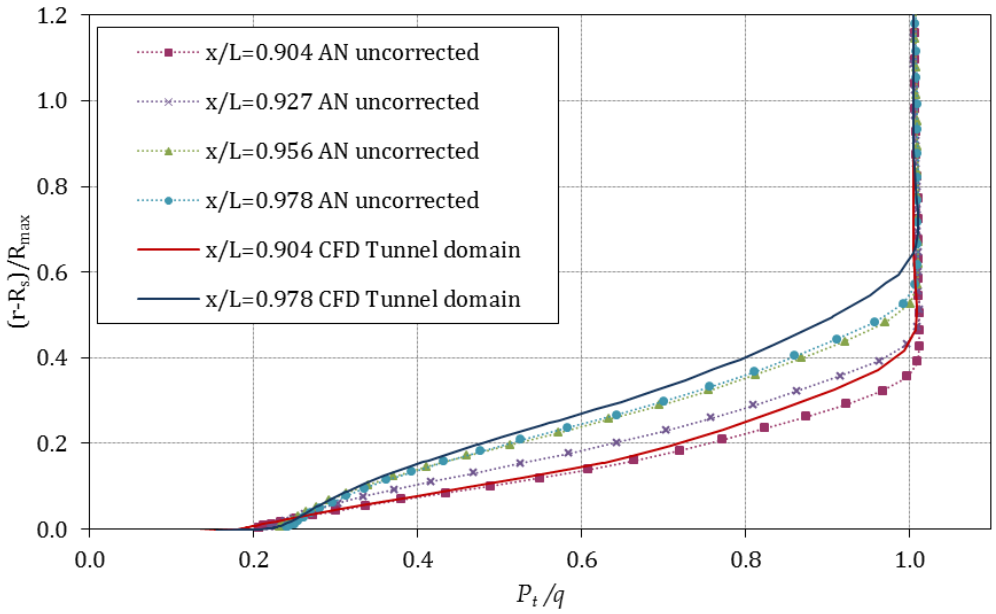

Figure 17: Total pressure boundary layer measurements on the SUBOFF model with AMC tunnel domain CFD results (Ellis et al. 2015) for Re=12×10^6.

Using CFD simulations it is possible to correct the blockage not just by how the free-stream is accelerated but also by the change in boundary layer shape. The boundary layer profile is affected by the combination of an accelerated free-stream and the artificially high pressure gradients. Figure 18 shows how rescaling the velocity by the free stream would result in an oversimplification of the blockage effect, particularly close to the hull boundary. This correction is better performed by rescaling the velocity for each location measured as follows:

$$\frac{u_i}{U}_{corrected} = \left(\frac{u_i}{U_\infty}\right)_{measured} \left(\frac{u_{i,\mathrm{LB}}}{u_{i,tunnel}}\right)_{CFD} \tag{8}$$

The subscript *i* refers to a radial position, interpolated from the CFD data at the measured location.

The corrected boundary layer measurements are generally in good agreement with the open water CFD calculations. There is a small discrepancy between the corrected results and the DTRC results, which is most likely a small variance between facilities. The one exception is the DTRC results for *x/L*=0.904, which appear to have an unexpectedly low free-stream velocity, unmatched by any of the subsequent measurements.

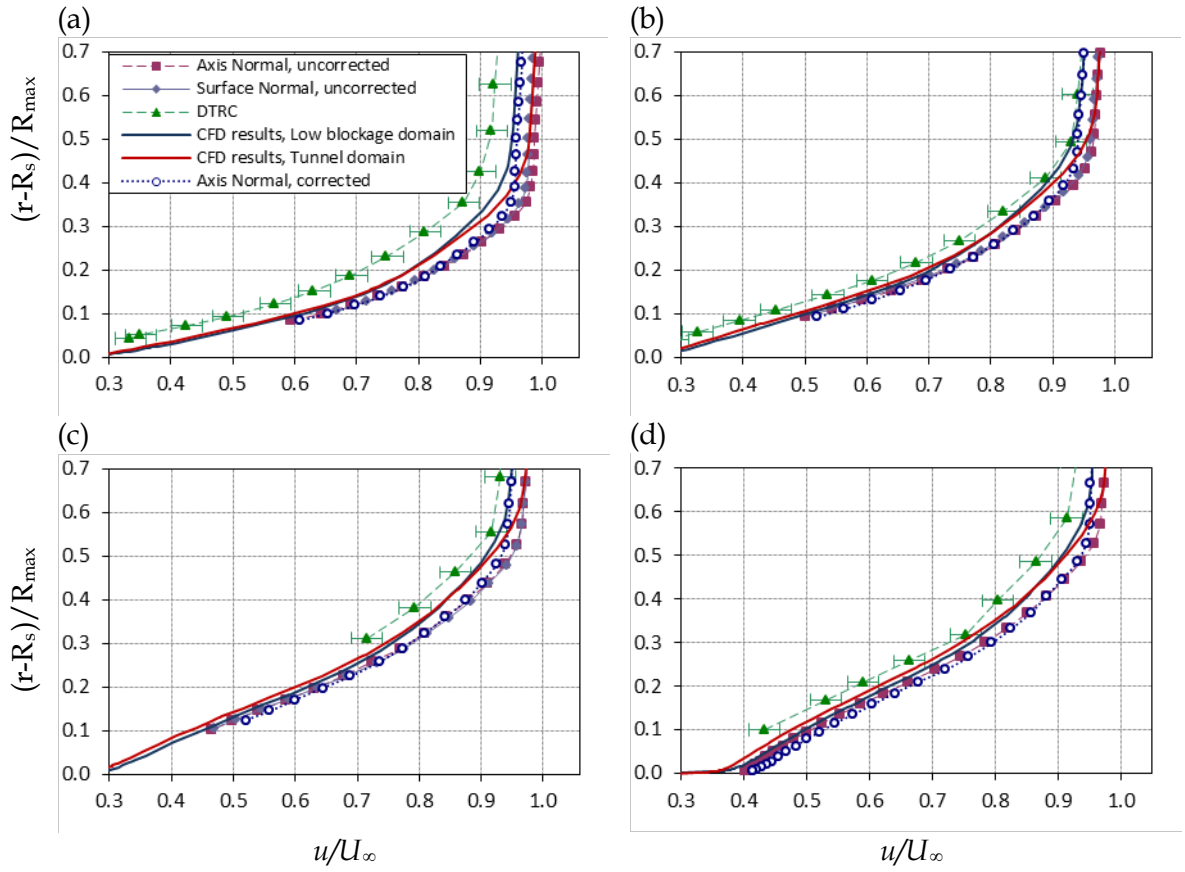

Figure 18: Normalised boundary layer velocities on the SUBOFF model shown over a smaller radial range at x/L=0.904 (a), 0.927 (b), 0.956 (c) and 0.978 (d) with DTRC measurements (Haung et al. 1989) and CFD (Ellis et al. 2015) for Re=12×10^6. Measurement uncertainty u/U∞±0.014

The calculated boundary layers are expected to be slightly thicker than their experimental counterparts as the turbulence model assumes the flow is turbulent along the entire length of the hull. For the measurements the boundary layer trip was placed at *x/L*=0.05 so the

length of turbulent flow for the measured flow is reduced and the boundary layer has had a slightly shorter length to thicken.

6.3.1 Turbulence intensity

The blockage will increase local velocities in the test section, which will generate greater shear stress in the boundary layer and hence greater turbulence intensity. This increase is apparent in a comparison of the turbulence intensity calculated using the low blockage domain and AMC tunnel test section domain. In keeping with the DTRC data, the turbulence intensity is referenced to the inlet velocity rather than the local velocity as described by Equation (9) and (10).

$$I = \frac{u'}{U_\infty} = \frac{1}{U_\infty}\sqrt{\frac{1}{3}\left(u_x'^{\,2} + u_y'^{\,2} + u_z'^{\,2}\right)} \tag{9}$$

Measurements at the DTRC facility were made using multi-axes hot film anemometry allowing them to resolve the turbulence components in each direction. Each of these can be considered a single component of the turbulence intensity (Equation (10]). The RANS turbulence model used in the CFD simulations does not determine turbulence component directions, thus the computed total turbulence intensity (Equation (9]) is shown in Figure 19.

$$I_x = \frac{u_x'}{U_\infty} = \frac{\sqrt{\overline{u_x'^{\,2}}}}{U_\infty} \tag{10}$$

The instantaneous total pressure is given by

$$P_T = \frac{\rho}{2}\left((u_x + u_x')^2 + \left(u_y + u_y'\right)^2 + (u_z + u_z')^2\right) + \bar{P}_S + p' \tag{11}$$

where P_T is the total pressure, $\bar{P}_S$ is the average static pressure and p' the fluctuating component of the static pressure. If the total head probe, using a squared off tip, is aligned with the flow to within approximately 10°, the total pressure will be correctly measured (Barlow et al. 1999). If $(u_x + u_x') \gg \left(u_y + u_y'\right), (u_z + u_z')$ and the probe is aligned with the x axis then only u_x' makes a significant contribution to the unsteady component measured by the probe. Thus when the probe is aligned with the x axis and if the unsteady component of the static pressure is assumed to be negligible,

$$u_x + u_x' \approx \sqrt{\frac{2\,(P_T - \bar{P}_S)}{\rho}} \tag{12}$$

The approximation of neglecting u_y', u_z' and p' should result in a small overestimation of u_x'. Figure 19 shows reasonable agreement for u_x' between the corrected results obtained in the present work and those from DTRC in the outer part of the boundary layer but a poorer comparison close to the hull boundary. This poor agreement may be due to the

reduction in the relative magnitude of u_x so that the condition $(u_x + u'_x) \gg (u_y + u'_y), (u_z + u'_z)$ is no longer true. The assumption in Equation (12) that the total head probe is only sensitive to the x component of the velocity will also result in an overestimation of u'_x as the total head probe will measure the total velocity vector if it is within a 15° cone angle of the probe tip's axis.

The blockage correction used for the turbulence measurements was based on the free-stream velocity rather than from a direct comparison of the results from the CFD simulations. The turbulence kinetic energy from which the turbulence intensity is derived is modelled in a RANS solver and may not be accurately determined. So, as with the skin friction correction, the turbulence measurements were corrected by rescaling the measured data based on the maximum velocity at the *x/L* positions obtained from the CFD simulations (Equation (13]).

$$I_{x,corrected} = \frac{u'_x}{U_\infty} = \left(\frac{u'_x}{U_\infty}\right)_{measured} \left(\frac{(u_{LB})_{max}}{(u_{tunnel})_{max}}\right)_{CFD} \tag{13}$$

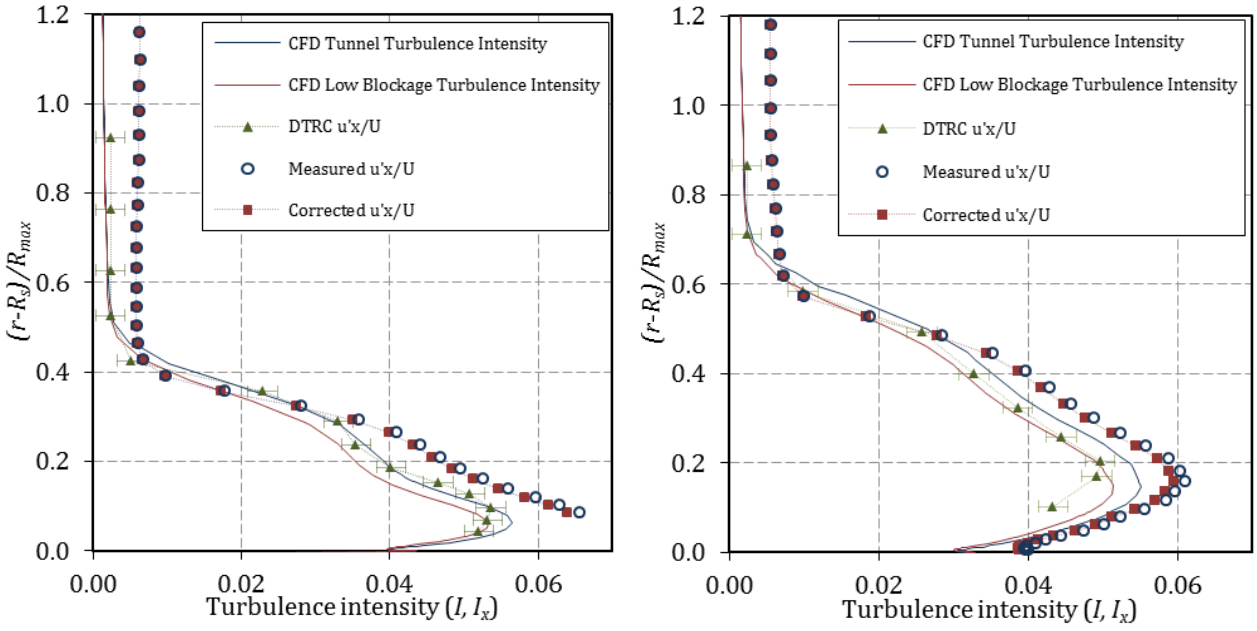

Figure 19: Turbulence intensity for the SUBOFF model at x/L=0.904 (left) and x/L=0.978 (right) compared to CFD models (Ellis et al. 2015) and the DTRC measurements (Haung et al. 1989) for Re=12×10⁶.

6.4 Wake velocity

The corrected wake velocity measurements are shown in Figure 20 for a series of circumferential measurement arcs. The measurement arcs were taken at *x/L*=0.978, the

propeller plane for this geometry. The wake from the support foils is evident at the 180° position, where 0° is defined along the y axis as in Figure 3. The corrected data shows close agreement between the bare hull circumferential surveys and the same points in the *x/L*=0.978 boundary survey, taken at 45°. This shows the repeatability of this measurement technique.

The same blockage correction used for the boundary layer surveys is applied to the wake velocity measurements. This consisted of applying a velocity scaling (Equation (*8*], as determined by the CFD models [Ellis et al. 2015).

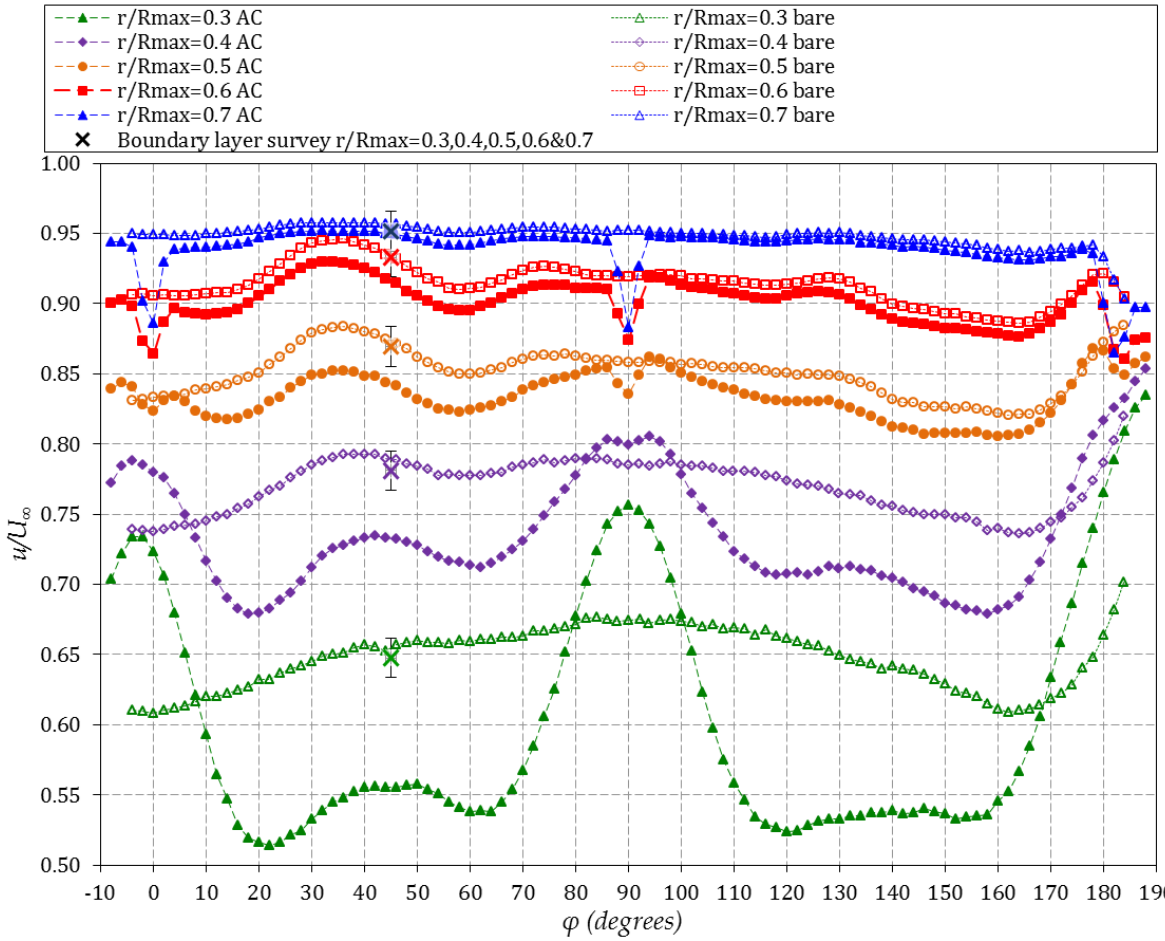

Figure 20: Corrected normalised velocities for the SUBOFF bare hull and bare hull with aft control surfaces at x/L=0.978 for Re=12×10^6. Measurement uncertainty of u/U∞ ±0.02 (Appendix A.4)

Post processing of the data revealed an 8% reduction in the free-stream total pressure for the measurements conducted when the aft control surfaces (AC) were fitted. This error proved to be a constant value and was most likely caused by an obstruction in the probe reference pressure system, resulting in an incorrect value of the static reference pressure ($P_{s,ref}$ from Equation (3]). An offset was applied to the aft control surface total pressure

measurements to compensate for this error prior to the blockage correction. For the effected data sets the offset was calculated such that the free stream reference total pressure was the same as the average of all other runs. The suspected obstruction is expected to result in only a small increase in uncertainty for these measurements as the cavitation tunnel maintains the test section static pressure and velocity within a small range. For more information see Appendix A.4.1.

The wake measurements show some unusual perturbations that would not be expected from a symmetric body at zero degrees incidence (Figure 21). The cause of this irregularity is uncertain but blockage due to the probe stem is suspected as it is the most apparent source of non-symmetry. The probe can be seen in Figure 7 taking a measurement at φ=0°. At this point the probe is extended over the hull and some degree of wake interaction is occurring between the hull and the stem. By contrast at φ=90° the probe is approaching the measurement location perpendicular to the hull and the interaction is reduced. An investigation of this error may be warranted using CFD if the 3D traverse is to be used longer term for measuring wakes near models with high blockage ratios.

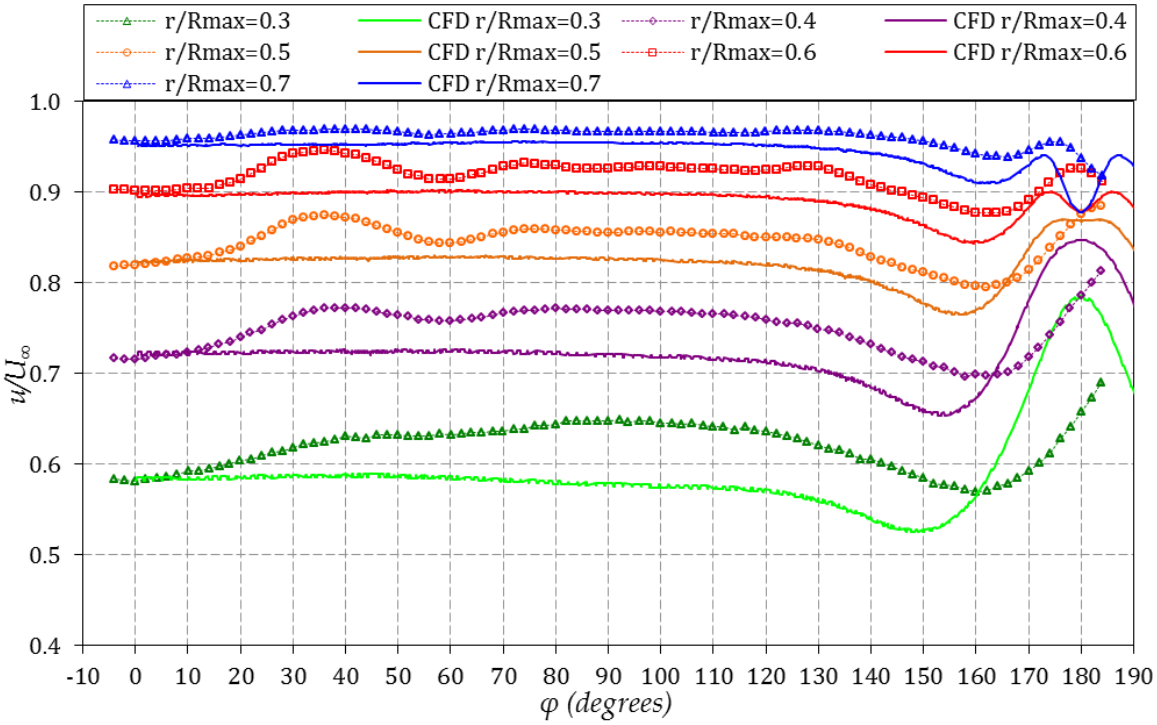

Figure 21: Wake velocities for uncorrected bare body experimental and CFD simulation of the SUBOFF model in the cavitation tunnel (Ellis et al. 2015). Measurement uncertainty of u/U_∞ ±0.02 (Appendix A.4)

7. Conclusions and Recommendations

The results presented in this report demonstrate that the AMC cavitation tunnel may be used to measure flow around submarine models at zero incidence. Additionally the results presented in this report demonstrate the validity of the CFD blockage correction techniques employed.

The surface pressure measurements for the SUBOFF model were successfully obtained and the blockage corrected results showed good agreement with the DTRC results. Good agreement was also obtained between the computational results for the SUBOFF model in the AMC tunnel and the measured results. The use of CFD simulations for blockage correction creates additional work but these simulations provide other advantages. The CFD simulations may be used to determine areas of interest, plan measurement locations and gain an insight into the flow structures at locations were measurements are unavailable.

Corrected skin friction measurements showed close agreement with the DTRC dataset demonstrating that the technique described in this report can be used to provide accurate measurements. The current application method for the Preston tube has subsequently been improved with a modified fairing and better techniques for adhering the tubes to the model. Erroneous points are easy to identify and, time permitting, may be remeasured to provide a full set of accurate measurements. With lessons learned from this testing future uses of the Preston tube mounted via a fairing should yield a greater proportion of successful applications.

Boundary layer velocities and turbulence intensities were measured with the fast response pressure probes. These results showed reasonable agreement with the DTRC measurements and the CFD simulations. Investigation into the unexpected perturbations in the velocity distribution shown in the circumferential surveys is warranted if this measurement technique is to be used in the future with large blockage ratios. Measurements from the single component fast response total pressure probe and static pressure probe were used to determine u'_x, however these measurements close to the surface overestimate u'_x. Single axis hot film anemometry would provide results with improved resolution that is valuable in thin boundary layers.

Overall, accurate measurements can be made on this size of submarine model in the AMC cavitation tunnel, but the blockage ratio requires significant correction, resulting in additional work. While this facility is suitable for measurements on this size model for zero angle of incidence, the advantage of larger facilities are evident; requiring smaller blockage corrections and allowing for testing at larger incidences. A submarine model with casing and fin would increase the blockage and require a more complex CFD mesh to determine the blockage correction. Any future full submarine measurements in the cavitation tunnel should aim for a reduced blockage ratio where possible. This may require careful consideration with regards to appendage Reynolds numbers.

8. Acknowledgements

The authors would like to acknowledge the high quality work of George Jeffs (QinetiQ Pty Ltd.) and Michael Popko (QinetiQ Pty Ltd). George undertook the detailed design of the SUBOFF model used in the AMC cavitation tunnel and Michael manufactured it.

9. References

1. Barlow, J. B., Rae, W. H. Jr., and Pope, A (1999) *Low speed wind tunnel testing*. 3rd ed. New York, Wiley-Interscience

2. Brandner, P.A. Lecoffre,Y., Walker. G.J. (2007) *Design Considerations in the Development of a Modern Cavitation Tunnel*; 16th Australasian Fluid Mechanics Conference, Gold Coast, Australia. 2-7 December 2007

3. Brown, K.C. and Joubert, P. N. (1969) *The measurement of skin friction in turbulent boundary layers with adverse pressure gradients*; Journal of Fluid Mechanics Vol. 35, Issue 4 pp. 737-757

4. Clarke, D.B. (2009) *Experimental and computational investigation of flow about low aspect ratio ellipsoids at transcritical Reynolds numbers.* [PhD Thesis] Launceston, University of Tasmania, Australia

5. Clarke, D.B., Butler, D., Ellis, C.L. and Brandner, P. (2016), *Hydrodynamic measurements on the Joubert hull in the AMC cavitation tunnel with CFD determined blockage corrections*, DST Group-TR- (in publication), Melbourne, Vic., Defence Science and Technology Group (Australia)

6. Ellis, C.L. Clarke, D.B., and Butler, D. (2016) *Complementary CFD studies of generic submarine model tests in the AMC cavitation tunnel,* DST Group-TR- (in publication), Melbourne, Vic, Defence Science and Technology Group (Australia)

7. Groves N. C., Huang T. T. and Chang M. S. (1989), *Geometric characteristics of DARPA SUBOFF models*, DTRC.SHD-1298-01, David Taylor Research Center, Bethesda, MD, USA

8. Haung, T. Liu, H.L. Groves, N. Forlini, T. Blanton, J. and Gowing, S.(1989) *Measurements of flows over an axisymmetric body with various appendages in a wind tunnel: the DARPA Suboff experimental program;* USA: David Taylor Model Test Basin

9. Head, M. R. and Ram V.V. (1971) *Improved presentation of Preston tube calibration*. India, Indian Inst. Tech. Kanpur Dept. Aero. Eng. AE-IO/1970. Aeronaut. Q.XXII, 3.

10. Kim, S. E., Choudhury, D., and Patel, B., 1999, "Computations of complex turbulent

11. flows using the commercial code Fluent," Modeling complex turbulent flows, M. D. Salas et al. eds., Kluwer Academic Publishers, pp. 259–276.

12. Patel, V.C. (1965) *Calibration of the Preston tube and limitations on its use in pressure gradients;* Journal of Fluid Mechanics, Vol 23 Issue 1 pp.185-208

This page is intentionally blank.

Appendix A: AMC measurement uncertainties

A.1. Surface pressure

Precision error (*Pr*)

The measurement precision error is defined as the 95% confidence interval of the sampled data points:

$$Pr = \frac{1.96\sigma}{\sqrt{N}}$$

Where P is the precision of the measurement, N is the number of independent samples and σ is the standard deviation of data.

The data was sampled at 1024 Hz for 10 s and filtered with a low pass 20 Hz, 2nd order Bessel filter. A conservative estimate of the number of statistically independent samples can be made by taking 50% of the filter frequency multiplied by the duration, in this case 100 samples.

Bias errors (*B*)

The Validyne differential pressure transducer is accurate to 0.25% full scale (-42 diaphragm FS=140 kPa). The sensor voltage was zeroed before each measurement set and referenced to the free-stream so the bias error was taken as 0.25% of the maximum dynamic pressure.

Uncertainty (*E*)

The total uncertainty, $E_{surface\ pressure}$, for the surface pressure measurement is defined as the root-sum-square of all uncertainty sources:

$$E_{surface\ pressure} = \sqrt{\sum B_i^2 + Pr^2} = \sqrt{B_{sensor}^2 + \left(\frac{1.96 * \sigma_P}{\sqrt{N}}\right)^2}$$

where B_i is the bias error from source i. For the surface pressure measurements the only identified source of bias errors was the pressure sensor linearity.

A.2. Incidence error

The surface pressure variation between the centre tappings and the port and starboard tappings was checked to ensure the model was aligned with the test section flow (Figure A1). There were slight differences but they were found to be well within the total measurement error ($C_{P\ error} \approx \pm 0.007$).

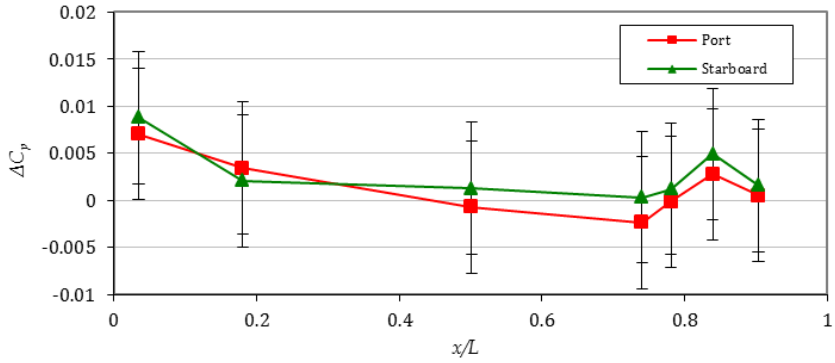

Figure A1: Port and Starboard measurements relative to the centreline measurements on the SUBOFF model. The results show the average of results for Reynolds numbers between 8×10⁶ and 18×10⁶ inclusive. Uncertainty Cp=0.007 (shown)

A.3. Skin friction

Measurement errors

The skin friction calculation was based on two separate pressure measurements, each with the same bias and random error sources as the surface pressure data. An additional error associated with interpolating the surface pressure to the Preston tube tip was included. The error associated with the interpolation of the surface pressure was estimated by repeating the interpolation process with CFD results. Computed surface pressure results were obtained at the locations where the surface pressure was measured. Interpolation was then used to determine the surface pressure at the location of the Preston tube tip. Comparing the surface pressure at the location of the Preston tube tip obtained directly from the CFD with the interpolation of the CFD results provides an estimate of the interpolation error. These errors were propagated through the calibration process to give error bands.

The pressure measurement uncertainty for the skin friction is defined as:

$$\mathrm{E_{pressure}} = \sqrt{\sum \mathrm{Bias}^2 + \mathrm{Precision}^2}$$

$$= \sqrt{\mathrm{E}^2_{\text{surface pressure}} + \mathrm{B}^2_{\text{interpolation}} + \mathrm{B}^2_{\text{sensor}} + \mathrm{Pr}^2_{\text{Preston}}}$$

Calibration errors

In addition to the pressure measurement errors the Preston tube calibration accuracy reduces when used in a pressure gradient. These errors have been quantified by Patel (1965) who provided limits for adverse and favourable gradients and Brown and Joubert (1969) who gave expanded limits for operating in adverse pressure gradients.

Patel's error bands:

1. Adverse pressure gradients:

   maximum error 3%: $0 < \Delta < 0.01, \frac{U_\tau d}{\nu} \leq 200$

   maximum error 6%: $0 < \Delta < 0.015, U_\tau d/\nu \leq 250$

2. Favourable pressure gradients:

   maximum error 3%: $0 > \Delta > -0.005, \frac{U_\tau d}{\nu} \leq 200, \frac{d}{dx(\Delta)} < 0$

   maximum error 6%: $0 > \Delta > -0.007, \frac{U_\tau d}{\nu} \leq 200, \frac{d}{dx(\Delta)} < 0$

where Δ (or p+) is defined as $\Delta = \frac{\nu}{\rho U_\tau^3}\frac{dp}{dx}$ and $U_\tau = \sqrt{\tau/\rho}$, d is the tube outside diameter, ν is the kinematic viscosity, ρ is the density.

A more detailed error approximation for high adverse pressure gradients was described by Brown and Joubert (Figure A2), where the pressure gradient, α, is defined as $\frac{1}{\rho}\frac{dp}{dx}$ (hence $\frac{\alpha\nu}{U_\tau^3} = \Delta$).

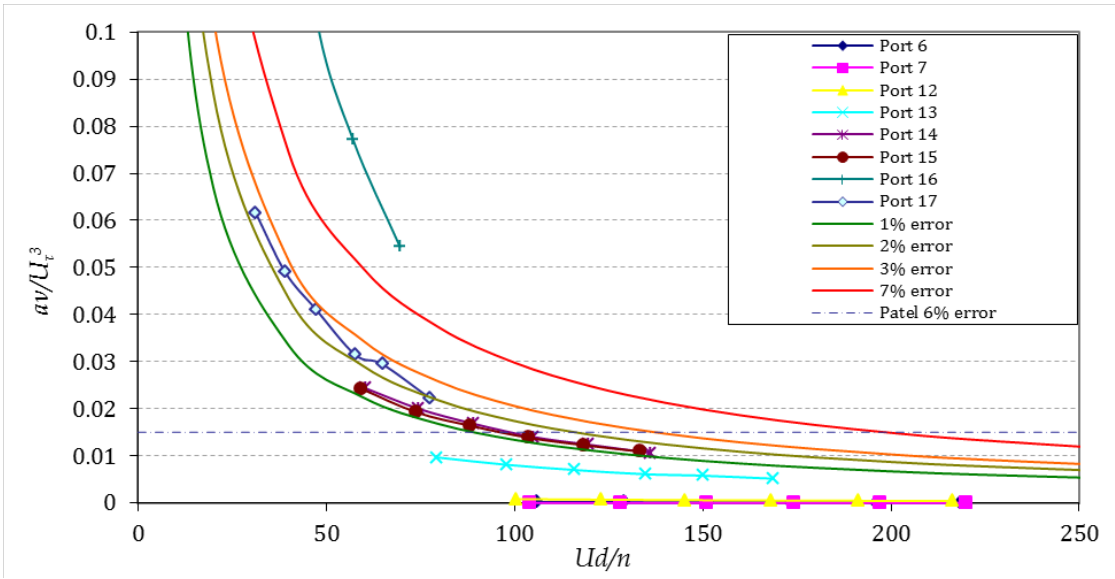

Figure A2: Brown & Joubert's (1969) errors for Preston tubes in an adverse pressure gradient for the SUBOFF model at Re=8×10^6 to 18×10^6

The measurement at Port 16 (x/L = 0.9) was found to be outside Brown & Joubert's limits for Preston tubes in an adverse pressure gradient (Figure A2) and was given a 20% error bar on top of other errors. This additional error most likely stems from a poorly applied Preston tube.

Table A1: Pressure gradient induced calibration errors

Port	6	7	8	9	10	11	12	13	14	15	16	17	18	19
Preston tube error	1%	1%	3%	3%	3%	3%	1%	1%	2%	2%	20%	3%	1%	3%

Total uncertainty (*E*)

These errors are combined with the pressure measurement errors, which were propagated through the calibration formulae to give the net error:

$$E_{skin\ friction} = \sqrt{\left(C_f * E_{grad}\right)^2 + \left(C_f\left(P + E_{pressure}\right) - C_f(P)\right)^2}$$

Where E_{grad} is the sum of the pressure gradient and boundary layer error given in Table A1 for an individual port.

A.4. Velocity measurements

Precision error (*Pr*)

The precision of the velocity measurement was taken as the 95% confidence interval of the measurements,

$$Pr = \frac{1.96\sigma}{\sqrt{N}}$$

Where N is the number of statistically independent samples and σ is the standard deviation of data. The data was sampled at 16384 Hz for 20 s and filtered with low-pass 2 kHz 1st order Bessel filter. A conservative estimate of the number of statistically independent samples can be made by taking 50% of the filter frequency multiplied by the duration, in this case 20000 samples.

Bias errors (*B*)

The Entran EPB-B01-7B-Z2 transducer has a 0.75% full scale error. The sensor output was digitally zeroed at the beginning of each test. By then exposing the probe to the known free-stream dynamic pressure the sensitivity of the probe across the free-stream dynamic pressure may be determined. Using this technique, the error is taken as 0.75% of the free-stream dynamic pressure.

$$B_{sensor} = 0.0075q$$

The static pressure probe exhibited slight velocity dependence. This was corrected by a linear relationship (Figure A3) between the static and dynamic pressure of dPs/dq=-0.0505. This relationship was an estimate with its own error, taken from the residuals as 10% of the correction.

$$B_{Ps} = 0.1\Delta Ps$$

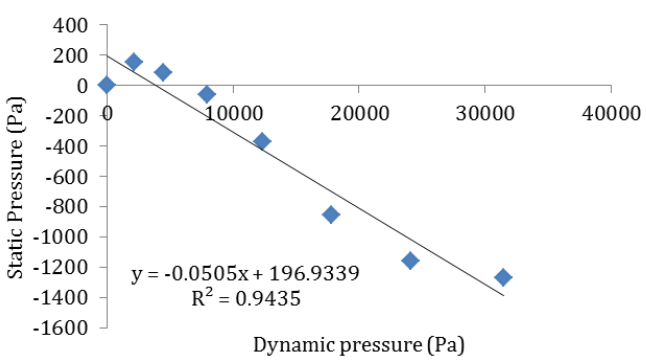

Figure A3: Static probe velocity dependence

The velocity dependence can then be applied to the data u/U as a multiplication constant by the following derivation.

Assuming a constant $\frac{dP_s}{dq}$ such that,

$$\frac{P_{sc}}{q} = \frac{P_s}{q} - \frac{dP_s}{dq}\frac{q_i}{q}$$

where P_{sc} denotes is the term corrected static pressure. Then if:

$$\frac{u_i}{U} = \left(\frac{P_t}{q} - \frac{P_{sc}}{q}\right)^{0.5}$$

substituting the result for $\frac{dP_s}{dq}$ into the above equation gives:

$$\frac{u_i}{U} = \left(\frac{P_t}{q} - \frac{P_s}{q} + \frac{dP_s}{dq}\frac{q_i}{q}\right)^{0.5}$$

and subtracting $\frac{u_i}{U}$ from both sides and squaring results in:

$$0 = \frac{P_t}{q} - \frac{P_s}{q} + \frac{dP_s}{dq}\frac{q_i}{q} - \frac{q_i}{q}$$

as $\left(\frac{u_i}{U}\right)^2 = \frac{q_i}{q}$. Rearranging results in:

$$0 = \frac{P_t}{q} - \frac{P_s}{q} - \frac{q_i}{q}\left(1 - \frac{dP_s}{dq}\right)$$

and expressing as a function of non-dimensional dynamic pressure

$$\frac{q_i}{q} = \frac{\left(\frac{P_t}{q} - \frac{P_s}{q}\right)}{\left(1 + \frac{dP_s}{dq}\right)}$$

Thus:

$$\frac{u_i}{U} = \sqrt{\frac{\left(\frac{P_t}{q} - \frac{P_s}{q}\right)}{\left(1 - \frac{dP_s}{dq}\right)}}$$

This static pressure offset is seen in Figure A4.

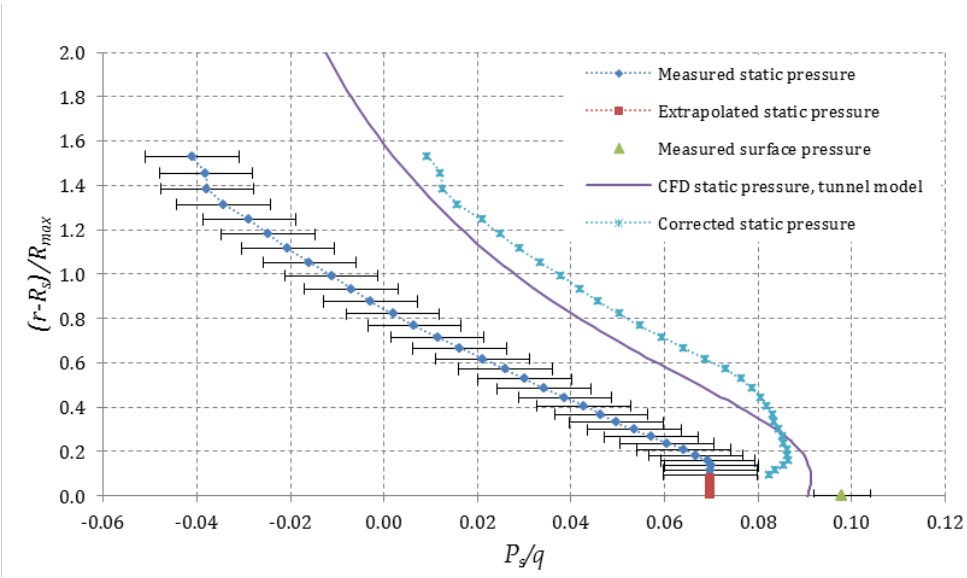

Figure A4: SUBOFF static pressure correction for x/L=0.98 boundary layer

The Entran sensor drift error was estimated from the free-stream reference taken at the start and end of every measurement series.

The precision error for the mean static pressure measurement at each location was included in the bias pressure errors.

The pressure bias errors, $B_{p/q}$, were converted to velocity bias errors by,

$$B_{u/U} = \sqrt{\sum B_{p/q}} \frac{du}{dp} = \frac{B_{p/q}}{2\sqrt{p/q}}$$

The probe positional uncertainty is typically less than 0.2 mm and does not contribute significantly to the overall measurement error.

Total uncertainty (*E*)

$$\textbf{Net error} = \text{RMS all errors} = \sqrt{\sum B_{u/U}^2 + Pr^2}$$

A.4.1 Probe blockage

A number of measurements were affected by a blockage in the fast response pressure probe's reference pressure line. The fault may have occurred when the bare model was removed from the tunnel and the aft control surface section replaced. This was an unfortunate oversight but a correctable one. The problem was determined to be a blockage in the static pressure line, as this is not only the most likely failure mode of this system but also explains the error seen. To check for such errors the probe was traversed to a free stream reference position before and after every circumferential survey. Table A2 shows

these free stream reference velocities. The distinction between the sets as well as the repeatability is clear.

Table A2 Freestream uncorrected reference velocities (u/U_∞) for SUBOFF wake surveys

	0.3	0.4	0.5	0.6	0.7
Bare start	1.017	1.016	1.014	1.014	1.014
Bare end	1.006	1.001	1.006	1.012	
AC start	0.980	0.974	0.971	0.971	0.973
AC end	0.975	0.967	0.969	0.971	0.973

Figure A5 shows the uncorrected circumferential wake surveys. This plot supports the assumption that the error is a constant velocity offset, such as might be expected from a constant pressure offset. There is no reason to suspect the sensors calibration is wrong, just that the zero reference is shifted. Also supporting this is the close agreement between the bare body circumferential surveys and the x/L=0.978 boundary layer survey interpolated to the same location, showing the probe sensitivity had not changed between measurement sets. The AC data was corrected by applying a total pressure offset to the raw pressure:

$$\Delta\frac{P_T}{q_\infty} = \left[\frac{u_{free}}{U_\infty}\right]^2_{Bare} - \left[\frac{u_{free}}{U_\infty}\right]^2_{AC}$$

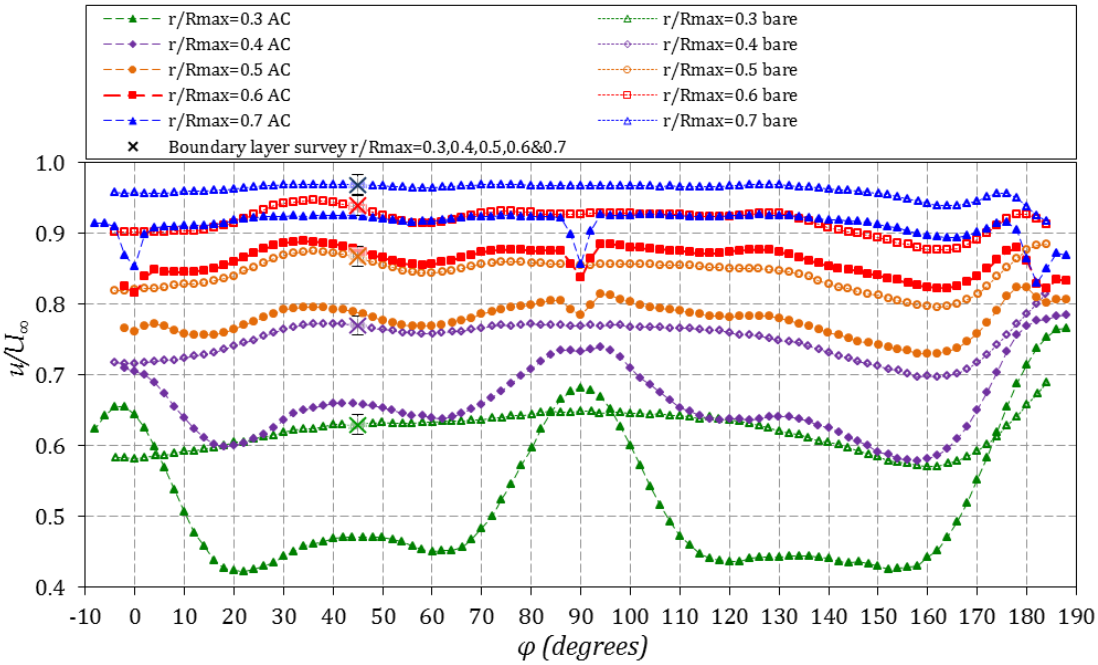

Figure A5: Uncorrected circumferential wake surveys for SUBOFF model at x/L=0.978 and Re=12×10^6

This page is intentionally blank.

Appendix B: Corrected hull data

B.1. Surface pressure

Port No.	X/L	C_p Re=12×10^6	Port No.	X/L	C_p Re=12×10^6
P0	0.000	1.012	P11	0.781	-0.219
P1	0.035	-0.166	P11P	0.781	-0.219
P1P	0.035	-0.160	P11S	0.781	-0.218
P1S	0.035	-0.158	P12	0.805	-0.197
P2	0.070	-0.099	P13	0.840	-0.061
P3	0.105	-0.068	P13P	0.840	-0.058
P4	0.181	-0.103	P13S	0.840	-0.056
P4P	0.181	-0.100	P14	0.857	0.017
P4S	0.181	-0.101	P15	0.873	0.079
P5	0.237	-0.043	P16	0.904	0.160
P6	0.402	-0.007	P16P	0.904	0.161
P7	0.501	-0.005	P16S	0.904	0.162
P7P	0.501	-0.005	P17	0.924	0.184
P7S	0.501	-0.003	P18	0.956	0.183
P8	0.601	-0.015	P19	0.978	0.137
P9	0.700	-0.046	P20	1.000	0.195
P10	0.741	-0.094			
P10P	0.741	-0.097			
P10S	0.741	-0.094			

B.2. Skin Friction

Port No.	x/L[#]	C_f Re=12×10^6
P6	0.396	0.00262
P7	0.495	0.00261
P8	0.594	0.00251
P9	0.693	0.00260
P10	0.734	0.00273
P11	0.775	0.00312
P12	0.798	0.00253
P13	0.833	0.00163
P14	0.851	0.00096
P15	0.866	0.00095
P16	0.897	0.00016
P17	0.918	0.00028
P18	0.950	0.00037
P19	0.972	0.00074

[#] Note: x/L location listed is for the measurement location at the Preston tube tip, 10mm upstream of the port location.

DEFENCE SCIENCE AND TECHNOLOGY GROUP DOCUMENT CONTROL DATA	1. DLM/CAVEAT (OF DOCUMENT)

2. TITLE	3. SECURITY CLASSIFICATION (FOR UNCLASSIFIED REPORTS THAT ARE LIMITED RELEASE USE (U/L) NEXT TO DOCUMENT CLASSIFICATION)
Benchmarking the AMC Cavitation Tunnel for Hydrodynamic Measurements on Submarine Models with CFD Determined Blockage Corrections	Document (U) Title (U) Abstract (U)
4. AUTHOR(S) Daniel Butler, David B. Clarke, Chris L. Ellis, Paul Brandner, Mohammed Kandoussi	5. CORPORATE AUTHOR Defence Science and Technology Group 506 Lorimer Street Fishermans Bend, Victoria, 3207, Australia

6a. DST GROUP NUMBER	6b. AR NUMBER	6c. TYPE OF REPORT	7. DOCUMENT DATE
DST-Group-TR-3358	AR-016-836	Technical Report	March 2017

8. OBJECTIVE ID	9.TASK NUMBER	10.TASK SPONSOR	11. MSTC	12. STC
[insert ID]	07/386	Sea 1000	Acoustic Signiture Management	Hydroacoustics

13. DOWNGRADING/DELIMITING INSTRUCTIONS	14. RELEASE AUTHORITY
To be reviewed three years after date of publication	Chief, Maritime Division

15. SECONDARY RELEASE STATEMENT OF THIS DOCUMENT

Approved for public release

OVERSEAS ENQUIRIES OUTSIDE STATED LIMITATIONS SHOULD BE REFERRED THROUGH DOCUMENT EXCHANGE, PO BOX 1500, EDINBURGH, SA 5111

16. DELIBERATE ANNOUNCEMENT

Australian Government personnel and others engaged in defence activities in Australia and their equivalent in USA, UK, Canada and NZ

17. CITATION IN OTHER DOCUMENTS Yes

18. RESEARCH LIBRARY THESAURUS

SUBOFF, blockage, submarine, cavitation tunnel, Reynolds Number

19. ABSTRACT

The widely studied generic submarine hull form SUBOFF was used to benchmark the use of the Australian Maritime College's (AMC) cavitation tunnel for hydrodynamic measurements on submarine models. The measurements acquired at the AMC cavitation tunnel are a subset of those taken at the David Taylor Research Centre (DTRC), allowing direct comparison. The measurements were performed on a 1.54 m model for Reynolds numbers between 8 and 18 million. The measurements included surface pressure, skin friction, boundary layer velocities and a wake survey on the bare hull at zero degrees incidence. The large scale of the model relative to the tunnel resulted in a blockage ratio of 8.1%. The results were corrected using correction factors determined from Computational Fluid Dynamics (CFD) simulations, and displayed a high level of agreement with the DTRC results. The positive comparison showed that the AMC facility could be used for models of this size when combined with CFD based blockage corrections.